SOUTHERN PLAINS
TRANSPORTATION CENTER

Development of Novel Analysis Model for Foundations Subjected to Combined Torsional and Lateral Loads Due to High Wind

Hoyoung Seo, Ph.D., P.E.
Junyoung Ko, Ph.D.
Suranga Gunerathne, Ph.D.

SPTC15.5-03-F

Southern Plains Transportation Center
201 Stephenson Parkway, Suite 4200
The University of Oklahoma
Norman, Oklahoma 73019

DISCLAIMER

The contents of this report reflect the views of the authors, who are responsible for the facts and accuracy of the information presented herein. This document is disseminated under the sponsorship of the Department of Transportation University Transportation Centers Program, in the interest of information exchange. The U.S. Government assumes no liability for the contents or use thereof.

TECHNICAL REPORT DOCUMENTATION PAGE

1. REPORT NO.	2. GOVERNMENT ACCESSION NO.	3. RECIPIENTS CATALOG NO.
SPTC15.5-03-F		

4. TITLE AND SUBTITLE	5. REPORT DATE
Development of Novel Analysis Model for Foundations Subjected to Combined Torsional and Lateral Loads Due to High Wind	October 2, 2018
	6. PERFORMING ORGANIZATION CODE
7. AUTHOR(S)	8. PERFORMING ORGANIZATION REPORT
Hoyoung Seo, Junyoung Ko, and Suranga Gunerathne	
9. PERFORMING ORGANIZATION NAME AND ADDRESS	10. WORK UNIT NO.
Texas Tech Center for Multidisciplinary Research in Transportation Texas Tech University Box 41023 Lubbock, Texas 79409	11. CONTRACT OR GRANT NO. DTRT13-G-UTC36
12. SPONSORING AGENCY NAME AND ADDRESS	13. TYPE OF REPORT AND PERIOD COVERED
Southern Plains Transportation Center 201 Stephenson Pkwy, Suite 4200 The University of Oklahoma Norman, OK 73019	Final June 2017 – May 2018
	14. SPONSORING AGENCY CODE

15. SUPPLEMENTARY NOTES

University Transportation Center

16. ABSTRACT

In this study, we perform a nonlinear finite element analysis (FEA) for a circular foundation in an undrained clay under combined loading of a torque and a lateral load. To determine collapse loads, the displacement-controlled swipe loading path method is employed in FEA. Analysis results are presented in the form of failure envelopes as a function of embedment depth ratio for various definitions of ultimate lateral capacity. Results from FEA clearly show that lateral capacity is reduced by the concurrent application of torsion, and the reduction effects are quantified as a function of torque-to-lateral load ratio.

Based on the insights gained from FEA, we further develop a novel analysis model through analytical approach. Governing differential equations for a circular foundation, embedded in a layered soil, subjected to a combination of lateral and torsional loads are derived based on energy principles and variational calculus; a total of six, interdependent differential equations are obtained. We develop a numerical algorithm to solve the interdependent differential equations and test the algorithm under individual loading components, which shows excellent agreements with those from previous studies and FEA. A full implementation of the solution algorithm for combined loading case can be done as a future study. Furthermore, the analysis model developed in this study can be regarded as a groundwork for more advanced models such as nonlinear analysis model that considers degradation of soil modulus using a piecewise-linear approach.

17. KEY WORDS	18. DISTRIBUTION STATEMENT
Foundations; Torsion; Lateral load; Finite element analysis; Variational principles	No restrictions. This publication is available at www.sptc.org and from the NTIS.

19. SECURITY CLASSIF. (OF THIS REPORT)	20. SECURITY CLASSIF. (OF THIS PAGE)	21. NO. OF PAGES	22. PRICE
Unclassified	Unclassified	63	

SI* (MODERN METRIC) CONVERSION FACTORS

APPROXIMATE CONVERSIONS TO SI UNITS

SYMBOL	WHEN YOU KNOW	MULTIPLY BY	TO FIND	SYMBOL
		LENGTH		
in	inches	25.4	millimeters	Mm
ft	feet	0.305	meters	m
yd	yards	0.914	meters	m
mi	miles	1.61	kilometers	km
		AREA		
in^2	square inches	645.2	square millimeters	mm^2
ft^2	square feet	0.093	square meters	m^2
yd^2	square yard	0.836	square meters	m^2
ac	acres	0.405	hectares	ha
mi^2	square miles	2.59	square kilometers	km^2
		VOLUME		
fl	fluid ounces	29.57	milliliters	mL
oz	gallons	3.785	liters	L
gal	cubic feet	0.028	cubic meters	m^3
ft^3	cubic yards	0.765	cubic meters	m^3
yd^3	NOTE: volumes greater than 1000 L shall be shown in m^3			
		MASS		
oz	ounces	28.35	grams	g
lb	pounds	0.454	kilograms	kg
T	short tons (2000 lb)	0.907	megagrams (or "metric ton")	Mg (or "t")
		TEMPERATURE (exact degrees)		
^oF	Fahrenheit	5 (F-32)/9 (F-32)/1.8	Celsius or	^oC
		ILLUMINATION		
fc	foot-candles	10.76	lux	lx
fl	foot-Lamberts	3.426	$candela/m^2$	cd/m^2
		FORCE and PRESSURE or STRESS		
lbf	poundforce	4.45	newtons	N
lbf/in^2	poundforce per square inch	6.89	kilopascals	kPa

APPROXIMATE CONVERSIONS FROM SI UNITS

SYMBOL	WHEN YOU KNOW	MULTIPLY BY	TO FIND	SYMBOL
		LENGTH		
mm	millimeters	0.039	inches	in
m	meters	3.28	feet	ft
m	meters	1.09	yards	yd
km	kilometers	0.621	miles	mi
		AREA		
mm^2	square millimeters	0.0016	square inches	in^2
m^2	square meters	10.764	square feet	ft^2
m^2	square meters	1.195	square yards	yd^2
ha	hectares	2.47	acres	ac
km^2	square kilometers	0.386	square miles	mi^2
		VOLUME		
mL	milliliters	0.034	fluid ounces	fl oz
L	liters	0.264	gallons	gal
m^3	cubic meters	35.314	cubic feet	ft^3
m^3	cubic meters	1.307	cubic yards	yd^3
		MASS		
g	grams	0.035	ounces	oz
kg	kilograms	2.202	pounds	lb
Mg (or "t")	megagrams (or "metric ton")	1.103	short tons (2000 lb)	T
		TEMPERATURE (exact degrees)		
^oC	Celsius	1.8C+32	Fahrenheit	^oF
		ILLUMINATION		
lx	lux	0.0929	foot-candles	fc
cd/m^2	$candela/m^2$	0.2919	foot-Lamberts	fl
		FORCE and PRESSURE or STRESS		
N	newtons	0.225	poundforce	lbf
kPa	kilopascals	0.145	poundforce per square inch	lbf/in^2

*SI is the symbol for the International System of Units. Appropriate rounding should be made to comply with Section 4 of ASTM E380. (Revised March 2003)

ACKNOWLEDGEMENTS

The authors thank the Southern Plain Transportation Center (SPTC) for their sponsorship of this study. The authors also thank Ms. Kim Harris for her administrative support throughout the project.

Development of Novel Analysis Model for Foundations Subjected to Combined Torsional and Lateral Loads Due to High Wind

Final Report

October 2018

by

Hoyoung Seo, Ph.D., P.E.
Assistant Professor
Department of Civil, Environmental, and Construction Engineering
Texas Tech University

Junyoung Ko, Ph.D.
Postdoctoral Research Associate
Department of Civil, Environmental, and Construction Engineering
Texas Tech University

and

Suranga Gunerathne, Ph.D.
Teaching Assistant Professor
Department of Engineering
East Carolina University

Southern Plains Transportation Center
201 Stephenson Pkwy, Suite 4200
The University of Oklahoma
Norman, OK 73019

TABLE OF CONTENTS

List of Figures

List of Tables

Executive Summary

This study numerically investigates the effect of combined torsional and lateral loading on the response of circular foundations. The research team performs a series of nonlinear finite element analysis (FEA) to determine collapse loads of drilled shafts in an undrained clay using the displacement-controlled swipe loading path method. As a validation of the finite element model, we compare the results from FEA under each individual component of load (i.e., a pure torque and a pure lateral load) against previous studies and theoretical values, which shows an excellent agreement. We further present the analysis results under combined lateral and torsional loading in the form of failure envelopes with various embedment depth ratios of foundations. Results from FEA clearly show that the lateral capacity of foundations is reduced by the concurrent application of torsion. We quantify such reduction effects as a function of torque-to-lateral load ratio and present the results in the form of design charts.

Based on the insights gained from FEA, we further develop a novel analysis model through analytical approach. With an assumption of linear elasticity, we derive governing differential equations for a circular foundation, embedded in a multilayered soil, subjected to a combination of lateral and torsional loads using energy principles and variational calculus. A total of six interdependent differential equations result from the derivation. To solve the interdependent differential equations, we develop a numerical algorithm using an iterative solution scheme and test the algorithm under each individual loading component. The results from our analysis model under individual loading components show very good agreements with those from previous studies and FEA. The solution algorithm developed in this study can be fully implemented for combined loading case and thorough benchmark runs can be performed as future studies. Furthermore, the analysis model developed in this study can be regarded as the groundwork for more advanced models such as nonlinear analysis model that considers degradation of soil modulus using a piecewise-linear approach. Because the new analysis model is applicable for a multilayered soil, a systematic parametric study can be also performed to investigate the soil layering effect and optimize foundation design.

CHAPTER 1. INTRODUCTION

1.1 PROBLEM STATEMENT

The three most important forces that need to be considered for design of transportation infrastructure are compression, tension, and shear. For cantilever mast-arm structures –– such as sign trusses, traffic signals, and mast-arm light poles —– subjected to high wind loads, torsion is a particular concern in addition to the three primary forces. Also, any transportation structure which is laterally loaded is prone to undergo some degree of torsion due to eccentricity of the applied load.

While there are considerable studies on torsional behavior of the structural elements of a superstructure, little attention has been paid to torsional behavior of a foundation surrounded by soil or rock. Most studies on behavior of foundations have focused on axial or lateral loading condition, and routine foundation design does not consider torsional behavior. Although there is a growing literature on the torsional behavior of foundations, these studies have focused on foundations subjected to pure torsion (Randolph 1981; Hache and Valsangkar 1988; Guo and Randolph 1996; Guo et al. 2007; Zhang 2010; Misra et al 2014; Li et al. 2017). However, the cantilever mast-arm structures are likely to impose a simultaneous loading of a torque and a lateral load on foundation due to their inverted L shapes. It has been reported that evaluating foundation stability against torsional and lateral load failures *separately* is not a safe practice (McVay et al. 2003). Unfortunately, no analysis models or design guidelines are available that can consider the combined effects of torsional and lateral loads on a foundation. Even, finite element analysis studies on foundations subjected to combined torsional and lateral loads are exceedingly rare.

In this study, we perform a nonlinear finite element analysis (FEA) for a circular foundation under combined loading of a torque and a lateral load. To determine collapse loads, the displacement-controlled swipe loading path method is employed. Analysis results are presented in the form of failure envelopes as a function of embedment depth ratio for various definitions of ultimate lateral capacity. Results from

FEA clearly show that lateral capacity is reduced by the concurrent application of torsion, and the reduction effects are quantified as a function of torque-to-lateral load ratio. We also derive governing differential equations for a circular foundation, embedded in a layered soil, subjected to a combination of torsional and lateral loads based on energy principles and variational calculus. We further develop a numerical algorithm to solve these differential equations and test the algorithm under individual loading components. A full implementation of the solution algorithm can lead to a development of a novel analysis model for load-displacement response of circular foundations under simultaneous action of a torque and a lateral load as a future study.

1.2 Background

Impact of wind loads on stability of infrastructure is a very important design consideration. According to International Building Code (IBC 2015) and Minimum Design Loads for Buildings and Other Structures: ASCE/SEI 7-10 (ASCE 2013), ultimate design wind speeds of 115 miles per hour (185 km per hour) are typical in Region 6 states (AR, LA, NM, OK, and TX) for common transportation infrastructures such as bridges, as shown in Figure 1.1(a). Figure 1.1(a) further shows that the ultimate design wind speeds along coastal areas in Louisiana and Texas are much greater than 115 mph (185 km per hour) due to hurricanes, and can be as high as 170 mph (274 km per hour). Many of the Region 6 states frequently experience tornadoes, and special structures must be designed to withstand very high wind speeds due to tornadoes. For example, FEMA (2007) recommends the wind speeds of at least 200 miles per hour (322 km per hour) in most areas of Region 6 states, except for New Mexico, for design of community tornado shelters [refer to Figure 1.1(b)].

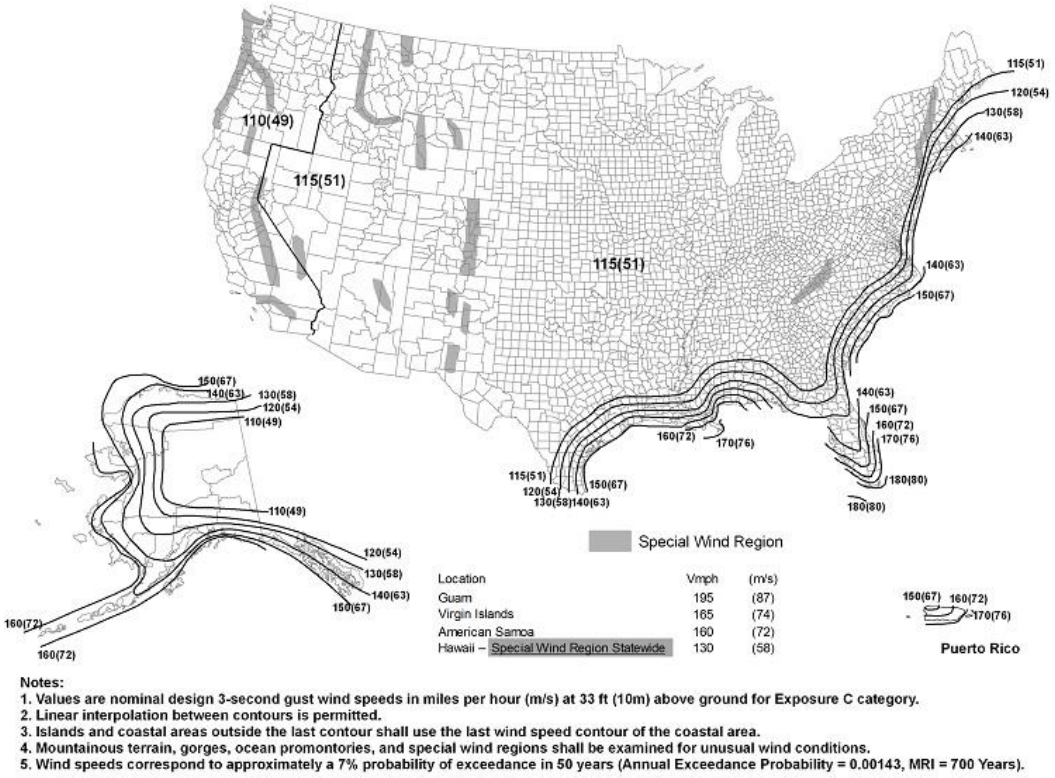

(a)

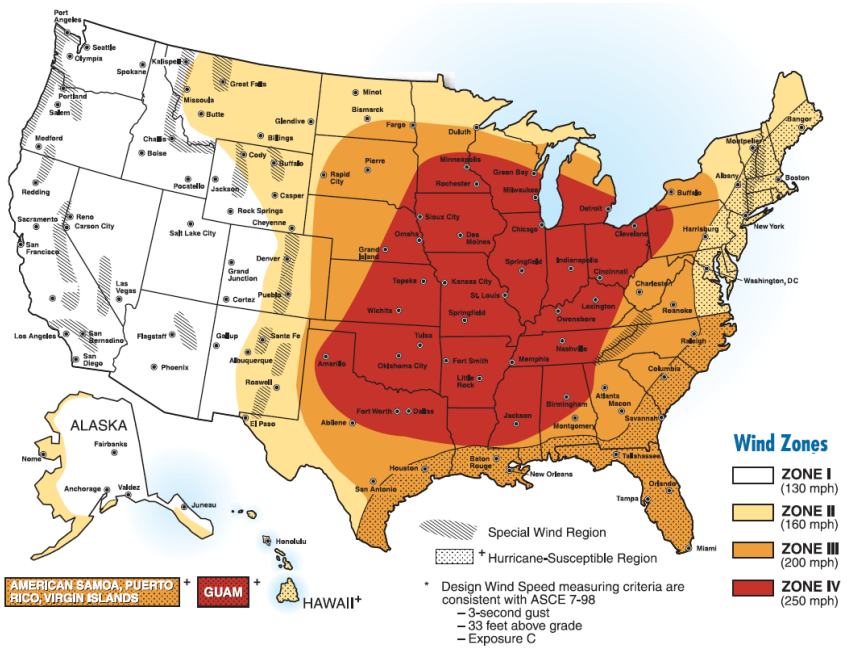

(b)

Figure 1.1 (a) Ultimate design wind speeds for Risk Category II buildings and other structures (IBC 2015) and (b) Design wind speeds for community shelters (FEMA 2007)

Large lateral loads induced by high winds will impose additional compression, tension, or shear forces on structural members and should be properly considered in design. Although these forces are the most common ones for typical structures, cantilever mast-arm structures (i.e., inverted L shape structures) and structures subjected to eccentric lateral load may develop significant torsional load on foundations in addition to these forces. Figure 1.2(a) shows a foundation of a cantilever overhead sign support structure subjected to the torsional and lateral loads simultaneously, and Figure 1.2(b) shows a failure of cantilever sign support structure along I-65 in Tennessee, allegedly caused by a “prolonged exposure to wind created by tractor trailer gusts (Beneberu et al. 2014).”

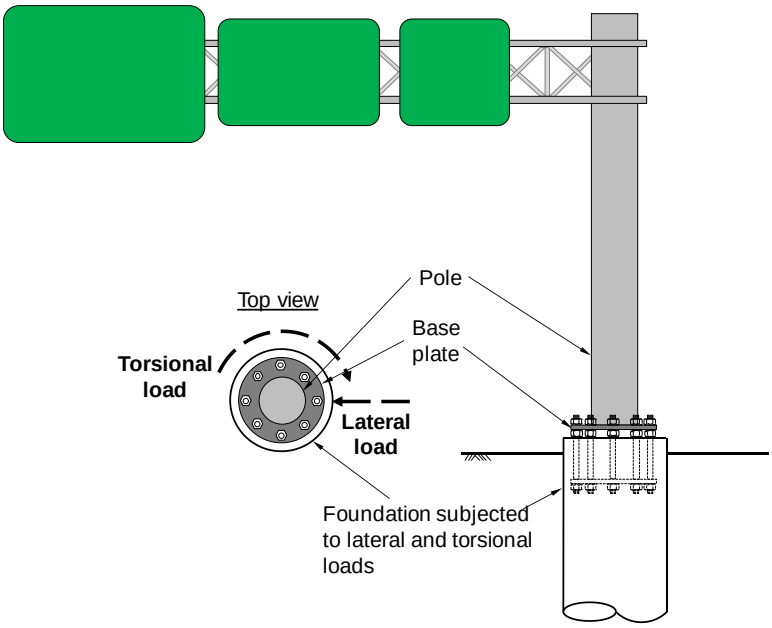

(a)

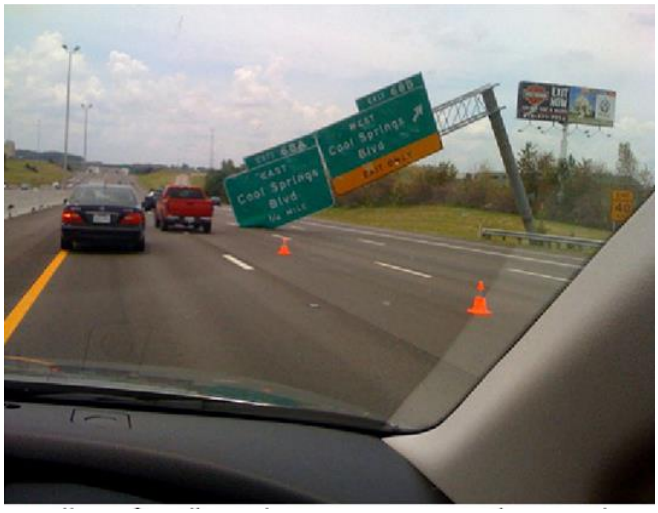

(b)

Figure 1.2 (a) A foundation of cantilever overhead sign support subjected to the torsional and lateral loads simultaneously and (b) failure of cantilever sign support structure along I-65 in Tennessee (Beneberu et al. 2014)

As mentioned previously, when the torsional loads are considered, the current geotechnical design practice is to evaluate stability of foundations against torsional and lateral load failures separately. The effects of a torque on lateral capacity of foundation (or vice versa) are barely understood. However, recent centrifuge tests and field tests performed by the researchers at University of Florida (McVay et al. 2003; Hu et al. 2006; Thiyyakkandi et al. 2016) have suggested that the lateral capacity of a drilled shaft is reduced when a torque and a lateral load are concurrently applied. This indicates that the current practice of separate evaluation of foundation stability against torsional and lateral load failures is not a safe practice. Because performing full-scale tests for various soil conditions with a wide range of foundation dimensions is practically and economically not feasible, there is a strong need to quantify the combined effects of lateral and torsional loads on foundation capacity through numerical analysis.

1.3 Objectives

The goal of this study is to numerically investigate the torsional and lateral resistances of circular foundations under combined loading. The main objectives of the study include:

(a) Performing nonlinear finite element analysis to determine failure envelopes under combined torsional and lateral loading
(b) Quantifying the effect of a torque on lateral capacity for various torque-to-lateral load ratios
(c) Deriving governing differential equations for load-displacement response of a circular foundation in a layered soil subjected to torsional and lateral loads
(d) Developing solution algorithm to solve the differential equations numerically.

CHAPTER 2. NUMERICAL MODELLING

2.1 Finite element model

The finite element analysis (FEA) is employed to investigate the behavior of a circular foundation subjected to under combined torsional and lateral loading using ABAQUS version 6.16 (Dassault Systèmes, 2016). The circular foundation, represented by a drilled shaft in this study, has a diameter D and a length L_p, embedded in a homogenous clay layer under undrained conditions. The diameter of the drilled shaft is set to be 1 m, and the effect of the embedment depth is investigated with three different lengths of the drilled shaft (L_p = 3, 5, and 10 m, corresponding to embedment depth ratios L_p/D of 3, 5, and 7, respectively). The L_p/D was limited to 10 because the embedment depth ratios of foundations for mast arm traffic sign and signal pole structures typically are smaller than 10. The linear elastic-perfectly plastic Tresca failure criterion is used to describe the clay behavior with an undrain shear strength of s_u and an undrained Young's modulus of $E_u = 500s_u$. To simulate the constant volume response during undrained loading, a Poisson's ratio ν_s of 0.49 was used for the clay along with zero degree of friction and dilation angles. The drilled shaft is modelled as a linear elastic material with a Young's modulus E_p = 25 GPa and Poisson's ratio ν_p = 0.3.

Eight-node brick elements with reduced integration (C3D8R) were used to model the drilled shaft and surrounding soil. A thin band of soil elements was used to capture the severe distortion close to the foundation without an interface model, as has been done by other researchers (Taiebat and Carter 2004 and Fan and Meng 2011). The domain boundaries are 30D (*i.e.*, 30 times the foundation diameter) in the horizontal direction and 2L_p (*i.e.,* 2 times the foundation length) in the vertical direction to minimize the boundary effect. The side boundary is horizontally fixed, and the base boundary is fixed in both horizontal and vertical directions. Analyses were performed under displacement-controlled conditions, where lateral and torsional displacements were applied at the foundation head and gradually increased.

2.2 Analysis results under a pure lateral load or a pure torque

The response of the drilled shaft under each individual component of load is presented first, followed by that under the combined loading.

2.2.1 Lateral response

The ultimate lateral capacity of a short foundation in an undrained clay can be obtained as follows:

$$H_{\max} = N_h L_p D s_u \tag{2.1}$$

where $H_{\max}$ = ultimate lateral capacity, L_p = foundation embedment depth, D = foundation diameter, s_u = undrained shear strength of clay, and N_h = lateral capacity factor. Deng and Carter (1999) suggested that N_h = 4.8 for a caisson with load applied at the foundation head, which is also a ground surface.

The load-displacement (H-w_r) responses of the drilled shafts obtained from FEA under lateral load with L_p = 3, 5, and 10 m are presented in Figures 2.1(a), (b), and (c), respectively.

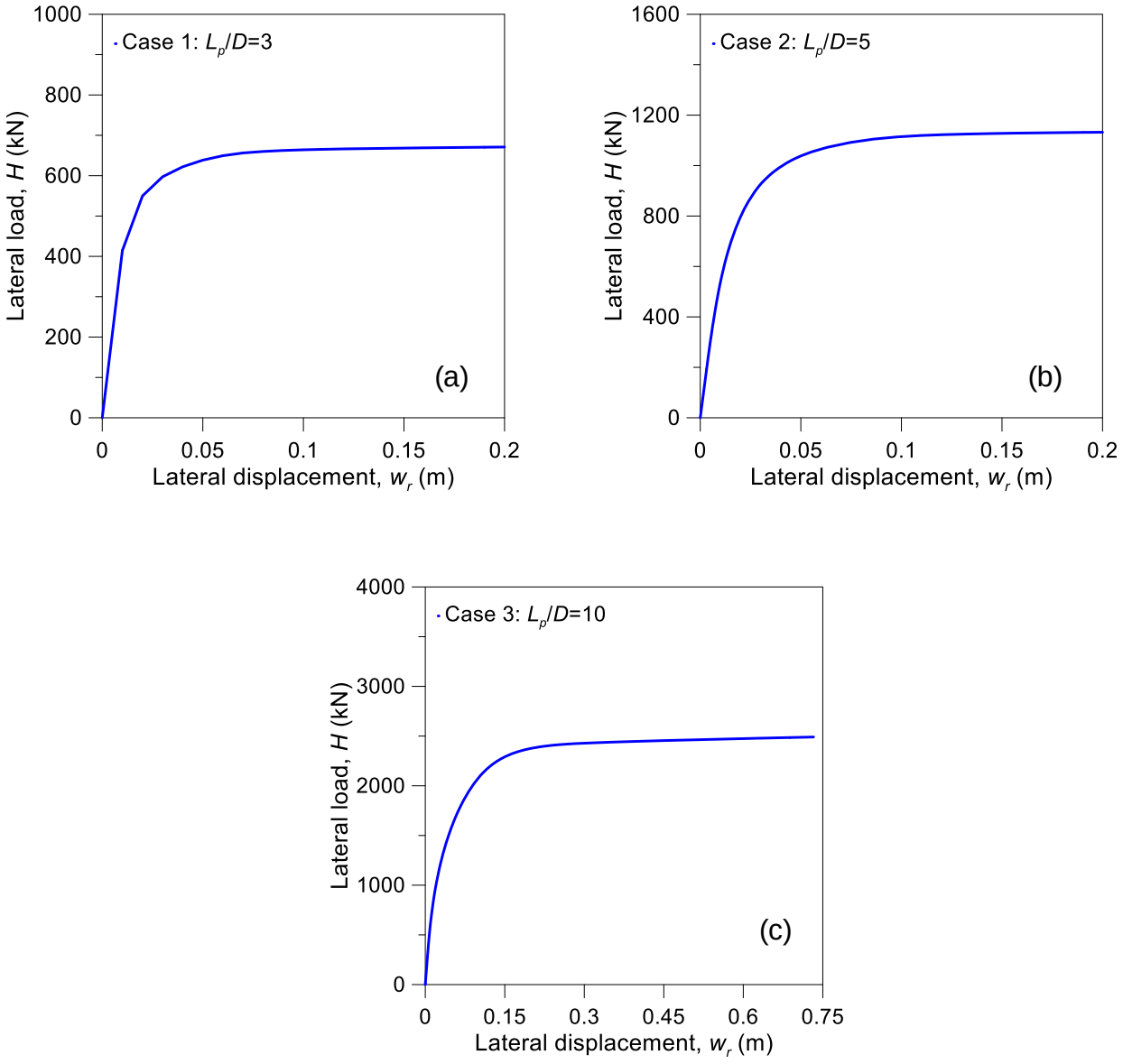

Figure 2.1 Load-displacement response under pure lateral loading: (a) L_p/D = 3, (b) L_p/D = 5, and (c) L_p/D = 10

The responses of drilled shafts under pure lateral load show nonlinear behavior, and it is clear that the lateral load approaches an asymptotic value at a large displacement. Although there are many criteria available in literature for determination of ultimate capacity of foundations under axial loading, such criteria are not well established for laterally loaded foundations. With the absence of widely accepted criteria for determination of ultimate lateral capacity H_{max}, we use four different ultimate capacity criteria in this study:

1) H_{max} is defined as a load H_{ult} after which the increase between two successive loads becomes less than 0.1%; this load is very close to the asymptotic value and might be considered as a true failure load;
2) H_{max} is defined as a load $H_{0.1D}$ at a lateral displacement corresponding to 10% of foundation diameter ($w_{r,ult}$ = 0.1D);
3) H_{max} is defined as a load $H_{0.05D}$ at a lateral displacement corresponding to 5% of foundation diameter ($w_{r,ult}$ = 0.05D);
4) H_{max} is defined as a load $H_{0.025D}$ at a lateral displacement corresponding to 2.5% of foundation diameter ($w_{r,ult}$ = 0.025D).

Graphical illustrations of each criterion are presented in Figure 2.2.

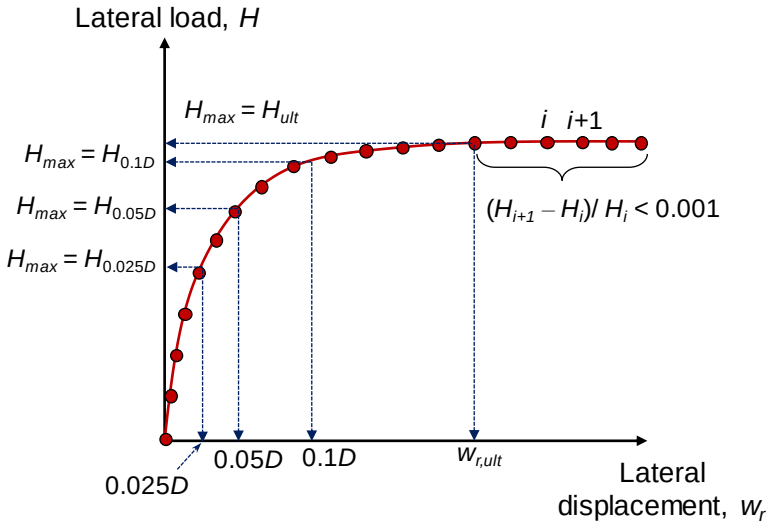

Figure 2.2 Graphical illustrations of ultimate lateral capacity criteria used in this study

Ultimate lateral capacities H_{max} determined using the aforementioned four criteria and their corresponding lateral displacements $w_{r,ult}$ are summarized in Table 2.1.

Table 2.1 Summary of ultimate lateral capacities under pure lateral loading for various ultimate capacity criteria

L_p/D	$H_{max} = H_{ult}$ (kN)	$w_{r,ult}$ (m)	N_h	$H_{max} = H_{0.1D}$ (kN)	$w_{r,ult}$ (m)	$H_{max} = H_{0.05D}$ (kN)	$w_{r,ult}$ (m)	$H_{max} = H_{0.025D}$ (kN)	$w_{r,ult}$ (m)
3	668	0.15	4.45	664	0.1	636	0.05	574	0.025
5	1130	0.18	4.52	1115	0.1	1038	0.05	871	0.025
10	2478	0.63	4.96	2078	0.1	1591	0.05	1136	0.025

Lateral capacity factors N_h from FEA were determined to be 4.45, 4.52, and 4.96 for foundations with L_p/D = 3, 5, and 10, respectively, using $H_{max} = H_{ult}$, and their values are given in Table 2.1. Despite slight differences, these lateral capacity factors are overall in good agreement with N_h = 4.8 obtained by Deng and Carter (1999) from their numerical analyses.

2.2.2 Torsional response

The relationship between a torque and an angle of twist for a straight cylinder with a fixed end is given as follows from elasticity theory:

$$\psi_p = \frac{TL_p}{G_p J_p} \tag{2.2}$$

where ψ_p = angle of twist, T = applied torque, G_p = shear modulus of the cylinder, and J_p = polar moment of inertia of cross section of the cylinder (see Figure 2.3).

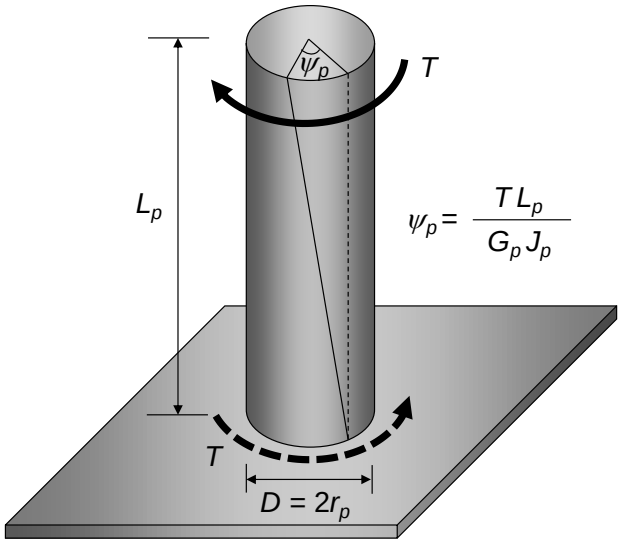

Figure 2.3 Angle of twist of a cylinder subjected to a torque

As shown in Figure 2.3, the angle of twist is greatest at the top of the cylinder and becomes zero at the base due to the fixed end condition. However, for a foundation embedded in soil, the angle of twist at the foundation base is not necessarily zero, especially for short foundations. Furthermore, when a torque is applied at the foundation head, frictional resistances develop 1) between the foundation and the surrounding soil along the shaft and 2) between the foundation base and the soil beneath it (refer to Figure 2.4). Therefore, an ultimate torsional capacity of a foundation in a homogeneous soil with an undrained shear strength s_u can be calculated as the sum of the shaft and base resistances as follows:

$$T_{\max} = T_s + T_b = (s_u \pi D L_p)\left(\frac{D}{2}\right) + \int_0^{D/2} (s_u)(2\pi r) dr = s_u \pi D^2 \left(\frac{L_p}{2} + \frac{D}{12}\right) \tag{2.3}$$

where T_{max} = ultimate torsional capacity.

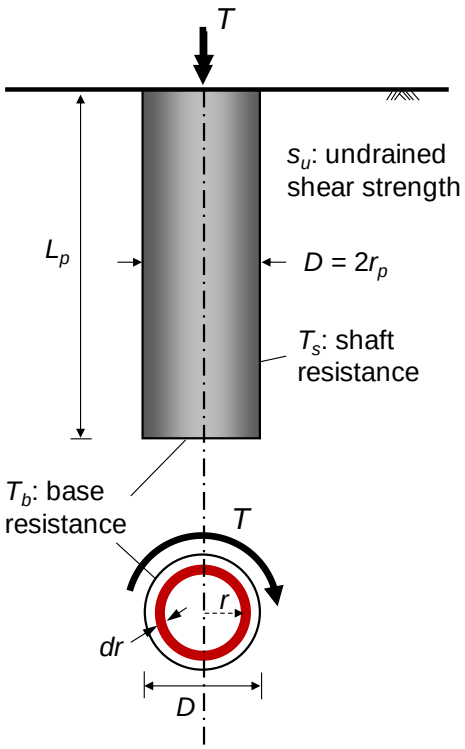

Figure 2.4 Torsional resistances of the foundation in soil

The torque-angle of twist (T-ψ_p) responses of the drilled shafts obtained from FEA under a pure toque with L_p = 3, 5, and 10 m are presented in Figures 2.5(a), (b), and (c), respectively. The torsional resistance from FEA linearly increases to its ultimate value and then remains constant after that, showing a behavior that is very close to linear-elastic, perfectly-plastic. Ultimate torsional capacity T_{max} and the corresponding angle of twist $\psi_{p,ult}$ from FEA were taken to be the values where a sudden change in slope was observed from the T-ψ_p plots. For comparison purposes, T-ψ_p responses from Eqs. (2.2) and (2.3) are also plotted in Figure 2.5, assuming that the angle of twist linearly increases until T reaches T_{max} and remain constants thereafter. Values of T_{max} and $\psi_{p,ult}$ obtained from the FEA and elasticity theory are summarized in Table 2.2

.

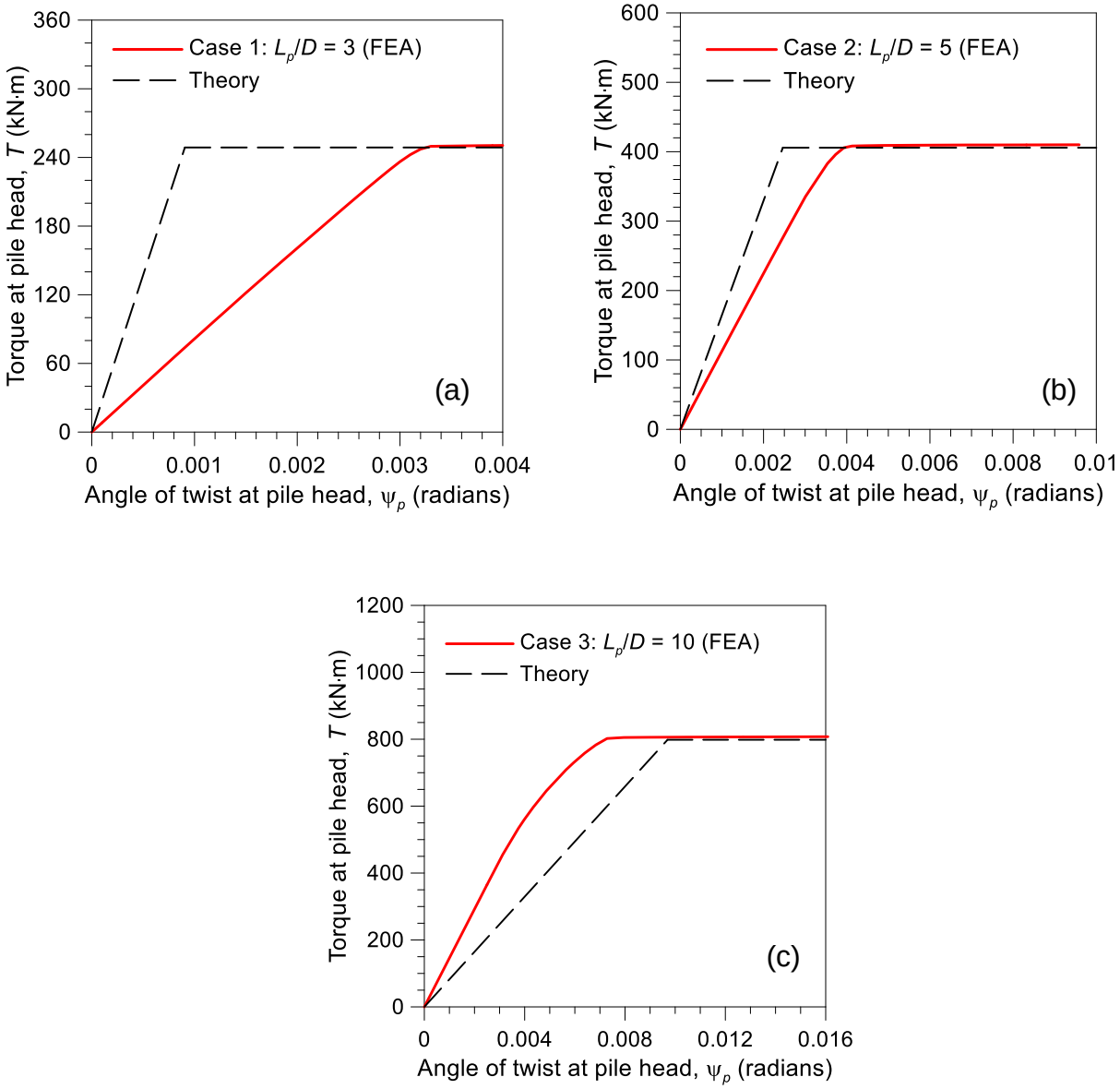

Figure 2.5 Torque-angle of twist response under pure torsional loading: (a) L_p/D = 3, (b) L_p/D = 5, and (c) L_p/D = 10

Table 2.2 Summary of ultimate torsional capacities under pure torsional loading

L_p/D [1]	T_{max} (kN-m) [2]	$\psi_{p,ult}$ (radian) [3]	T_{max} from Eq. (2.3) (kN-m) [4]	$\psi_{p,ult}$ from Eq. (2.2) with $T = T_{max}$ in Column [4] (radian) [5]	% difference in T_{max} [6]*
3	250	0.0033	249	0.0009	-0.4
5	408	0.0041	406	0.0025	-0.5
10	805	0.0080	798	0.0097	-0.9

* [6] = {[4]-[2]}/[4]x100%

Figure 2.5 and Table 2.2 show that T_{max} values from FEA and Eq. (2.3) are in excellent agreements, with the largest difference being only 0.9% for Case 3 (L_p/D = 10). However, the angle of twist $\psi_{p,ult}$ at the onset of the ultimate state show some discrepancies. For Cases 1 and 2 (L_p/D = 3 and 5, respectively), $\psi_{p,ult}$ values at the foundation head from Eq. (2.2) are smaller than those from FEA. On the contrary, $\psi_{p,ult}$ from Eq. (2.2) is greater than that from FEA for Case 3. This is because Eq. (2.2) assumes the full fixity condition at the cylinder base (i.e., ψ_p at the cylinder base is zero) but, in case of foundations, the foundation base is not fully fixed and the angle of twist at the foundation head is a summation of the rotation at the foundation base and angle of twist along the foundation shaft. As shown in Figure 2.6, the amount of angle of twist along the foundation shaft (i.e., the difference in ψ_p between the foundation head and base) is smaller than the values computed from Eq. (2.2) for all three cases because of resistances offered by the surrounding soil. However, foundation base undergoes certain levels of rotation as well and, consequently, the angle of twist at the foundation head depends on the amount of rotation at the foundation base, which is in turn influenced by the foundation embedment depth ratio. Figure 2.6, in conjunction with Figure 2.5 and Table 2.2, supports that the results from FEA well conform to the physics of the problem.

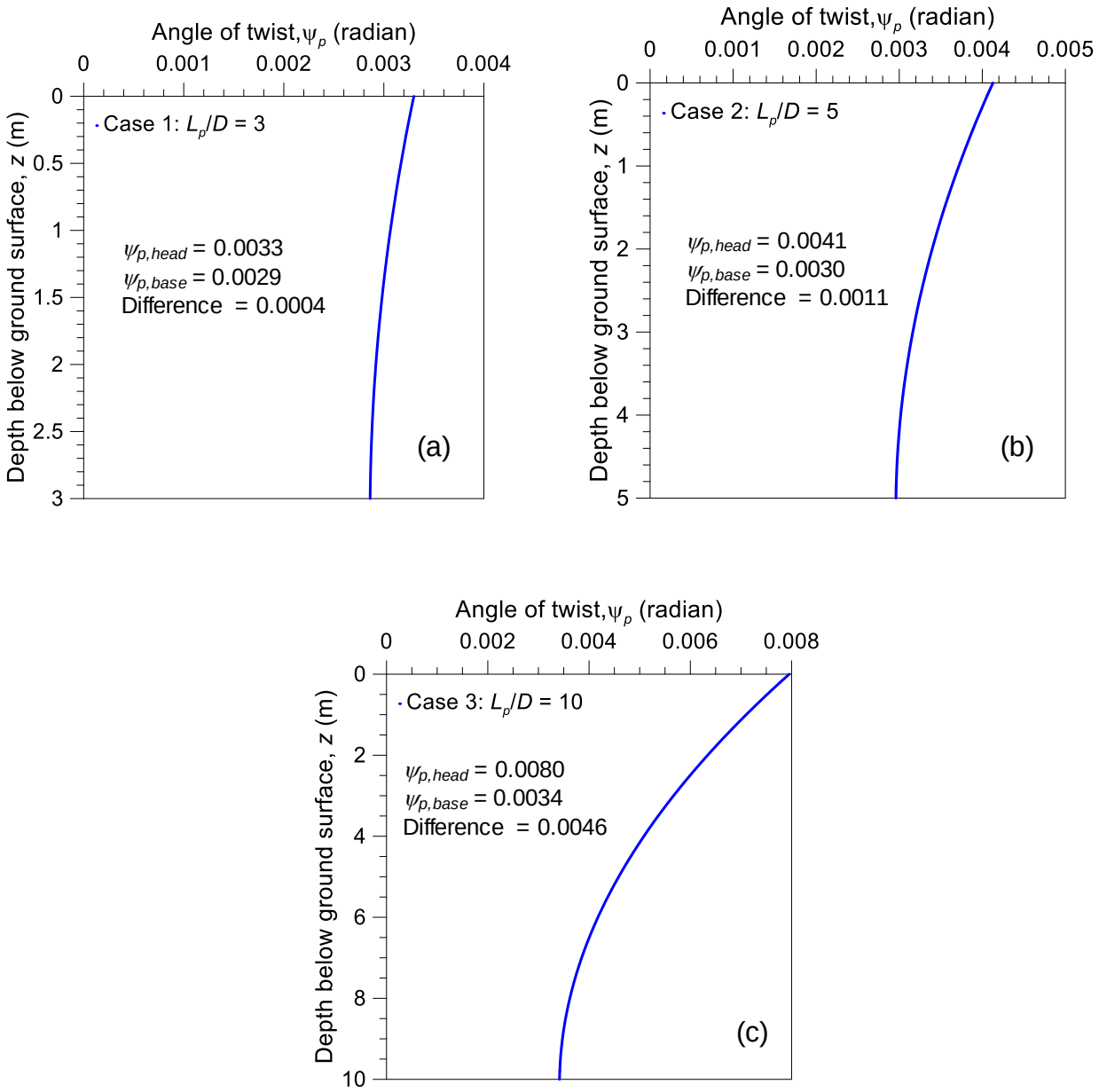

Figure 2.6 Angle of twist versus depth under pure torsional loading: (a) L_p/D = 3, (b) L_p/D = 5, and (c) L_p/D = 10

2.3 Analysis results under combined lateral and torsional loading

2.3.1 Numerical loading method

To determine the failure envelope under combined torsional and lateral loads, a two-staged, displacement-controlled swipe loading method, proposed by Tan (1990), was employed in our FEA. In the first stage, a lateral displacement w_r of the drilled shaft is prescribed and incrementally increased until the drilled shaft reaches an ultimate lateral load H_{max}. Once the ultimate lateral load and its corresponding lateral displacement $w_{r,ult}$ are determined, then an angle of twist ψ_p of the drilled shaft head is gradually increased in the second stage while keeping the lateral displacement constant at $w_{r,ult}$. The loading locus during the second stage can be considered as the failure envelop on the lateral-torsional load space. The displacement-controlled swipe loading method have been widely used to determine failure envelopes for isolated footings under various combined loading spaces (Gourvenec and Randolph, 2003; Vulpe et al., 2014; Lee et al 2016).

2.3.2 Failure envelopes under combined lateral and torsional loading

A series of finite element analyses was performed to obtain failure envelopes of the drilled shafts subjected to a combination of lateral and torsional loading, and they are

presented in

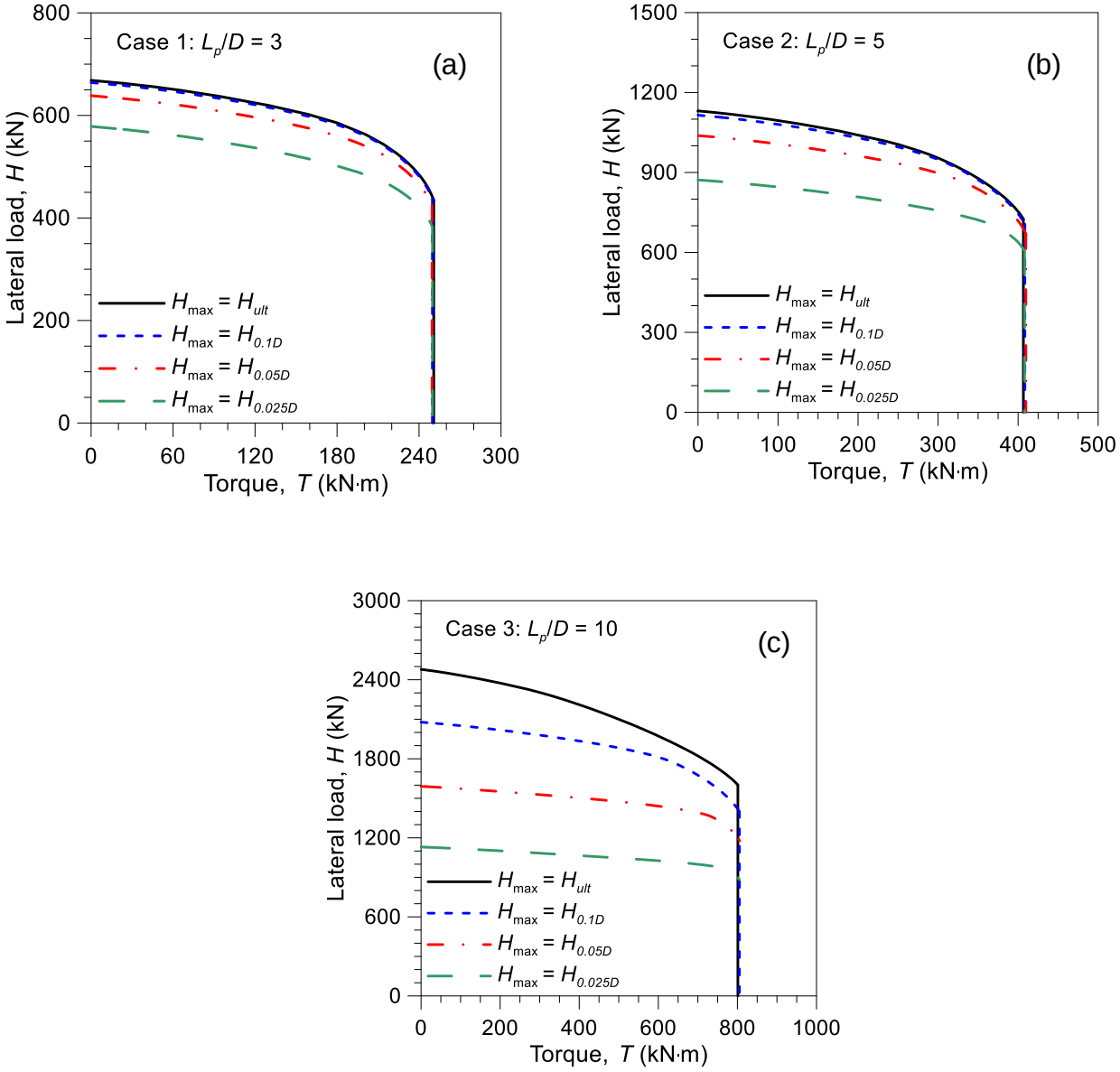

Figure 2.7. Note that four different definitions of H_{max} (i.e., $H_{max} = H_{ult}$, $H_{0.1D}$, $H_{0.05D}$, and $H_{0.025D}$), as presented in Figure 2.2 and Table 2.1, were used to plot the failure envelopes. Accordingly, a lateral displacement was gradually increased until reaching $w_{r,ult}$ for each definition of H_{max}, and then an angle of twist ψ_p of the drilled shaft was increased while keeping the lateral displacement constant at $w_{r,ult}$.

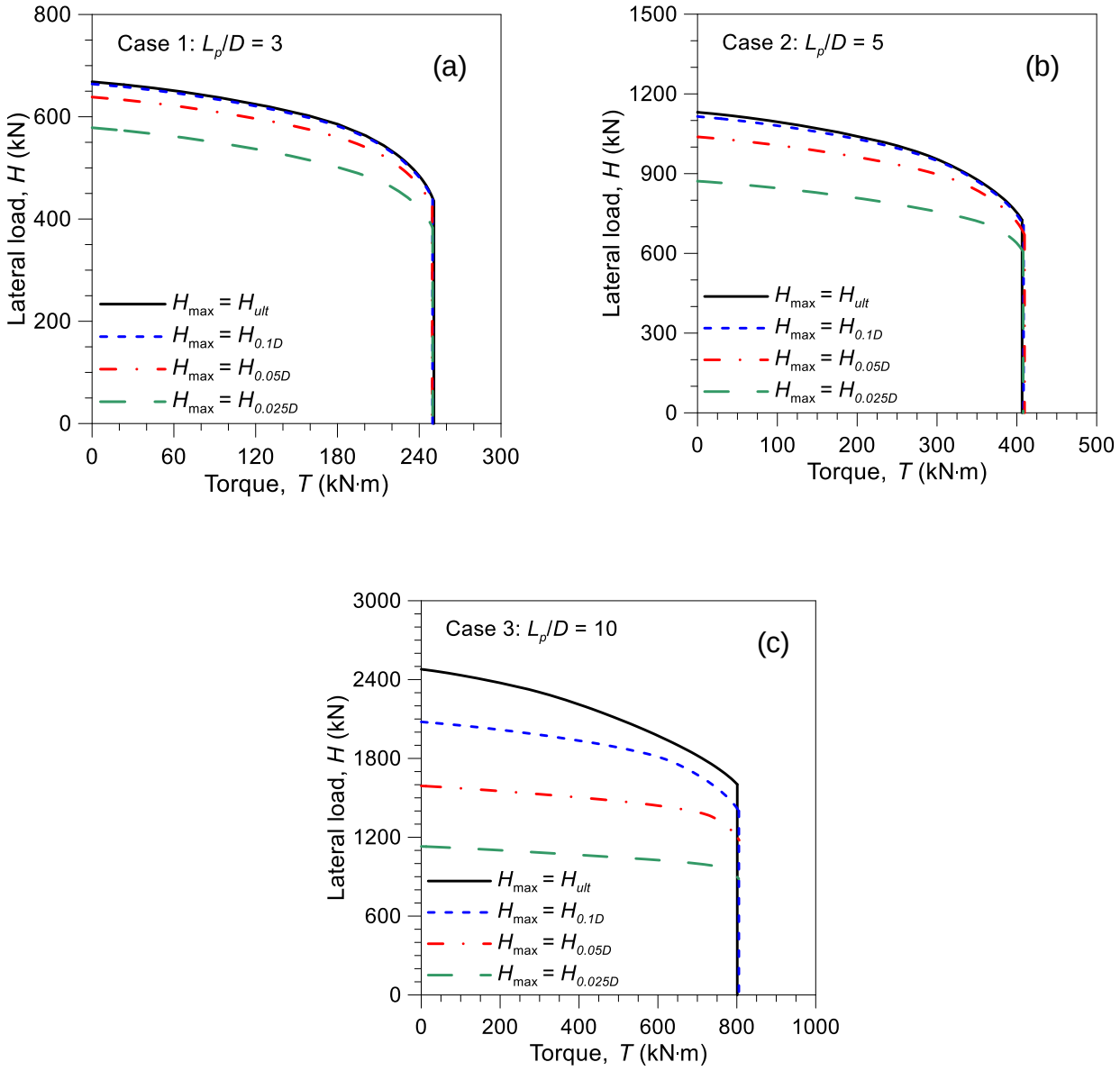

Figure 2.7 Failure envelopes in a lateral-torsional loading plane: (a) L_p/D = 3, (b) L_p/D = 5, and (c) L_p/D = 10

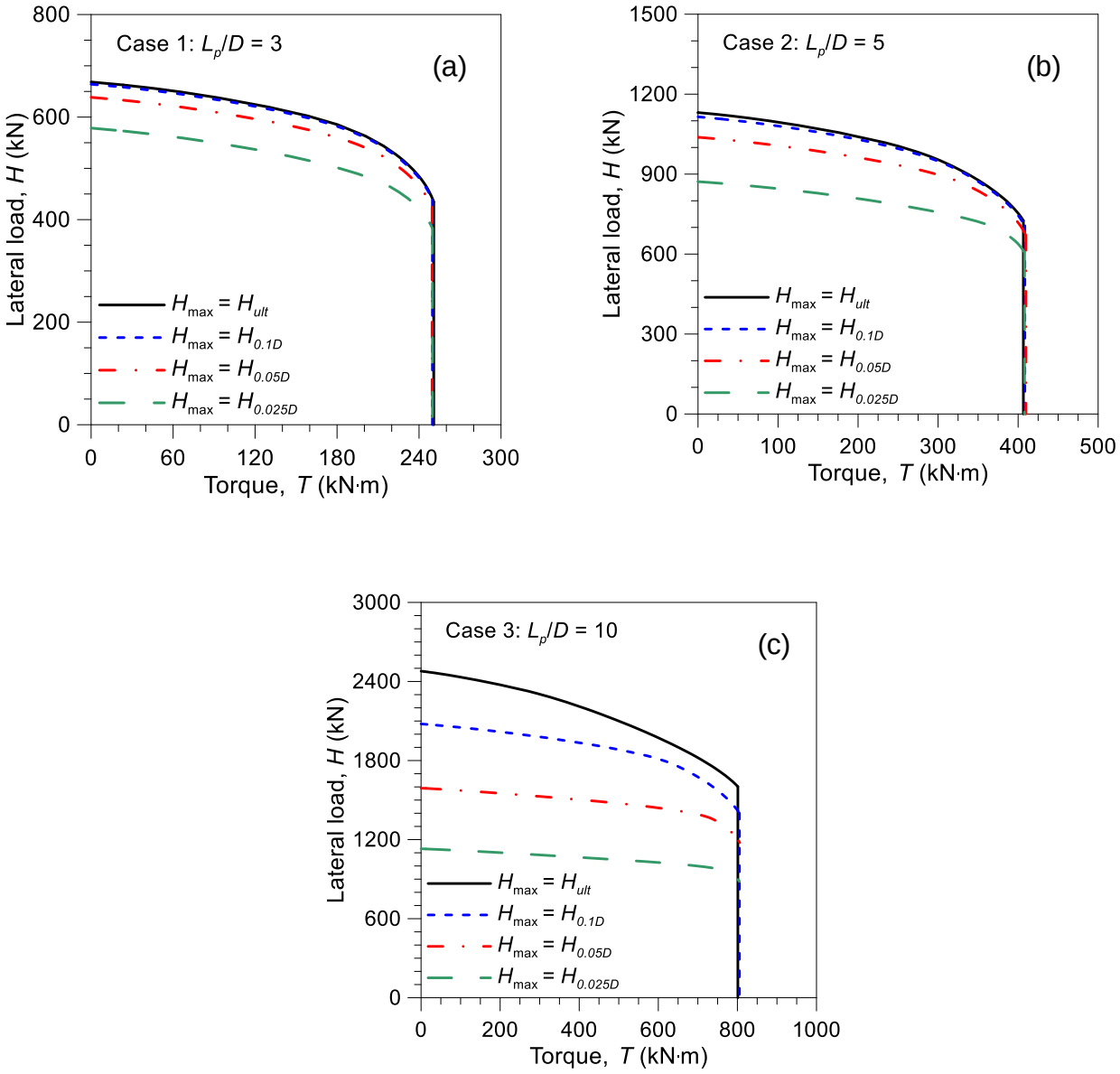

Figure 2.7 suggests that lateral loads at each failure envelope (i.e., equivalent to the maximum lateral capacity for each ultimate capacity criteria) decreases with an

increasing torsional load. The lateral and torsional loads shown in

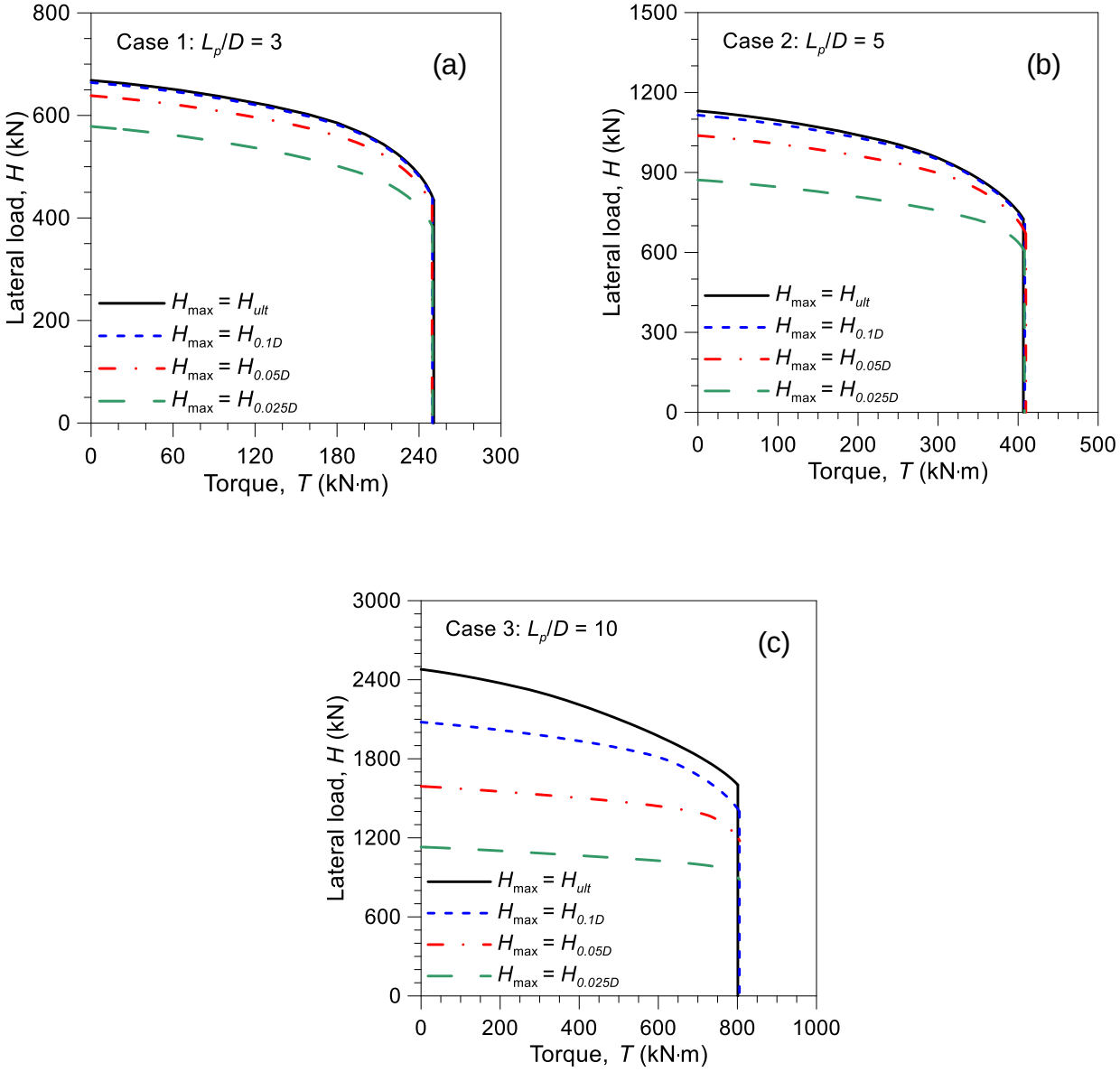

Figure 2.7 are normalized with respect to their maximum values H_{max} and T_{max} obtained under a pure lateral load and a pure torque, respectively, and the normalized failure envelopes are presented in Figure 2.8.

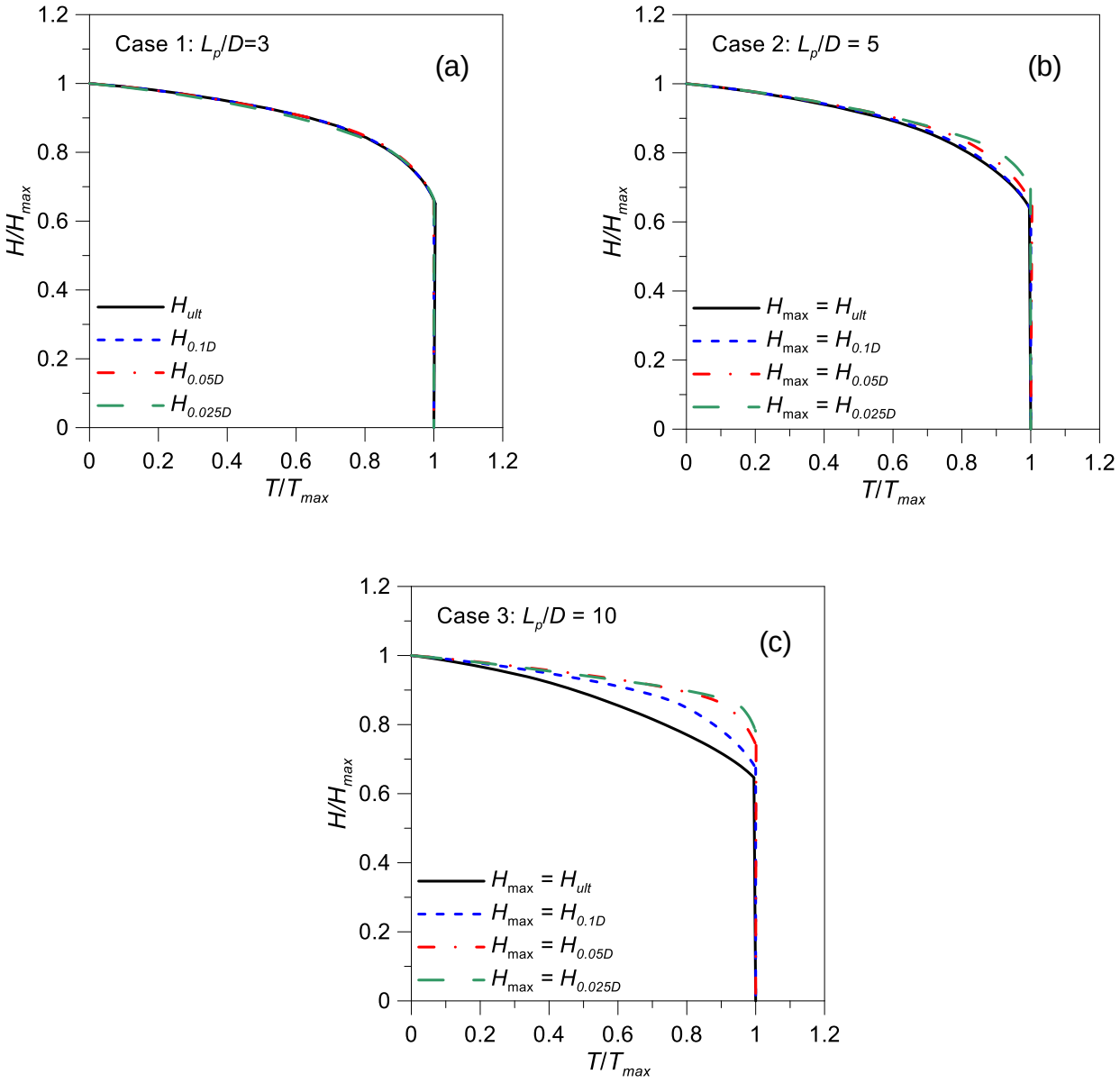

Figure 2.8 Failure envelopes in a lateral-torsional loading plane normalized with respect to H_{max} and T_{max}: (a) L_p/D = 3, (b) L_p/D = 5, and (c) L_p/D = 10

For L_p/D = 3, the normalized failure envelopes fall on top of each other regardless of definitions of H_{max}; this suggests that a single failure envelope may be used for a foundation with an embedment depth ratio less than 3. However, as the embedment depth ratio L_p/D increases, the normalized failure envelopes deviate from each other and do not justify the use of single failure envelope. Nonetheless, Figure 2.8 clearly

suggest that the lateral capacity decreases as the torsional load increases, and vice versa, regardless of how ultimate capacity is defined.

What could be more useful for design purpose is a chart that shows how much lateral capacity needs to be reduced for a given torque-to-lateral load ratio T/H. To achieve this, H/H_{max} versus T/H are plotted in Figure 2.9 using the torsional and lateral loads presented in

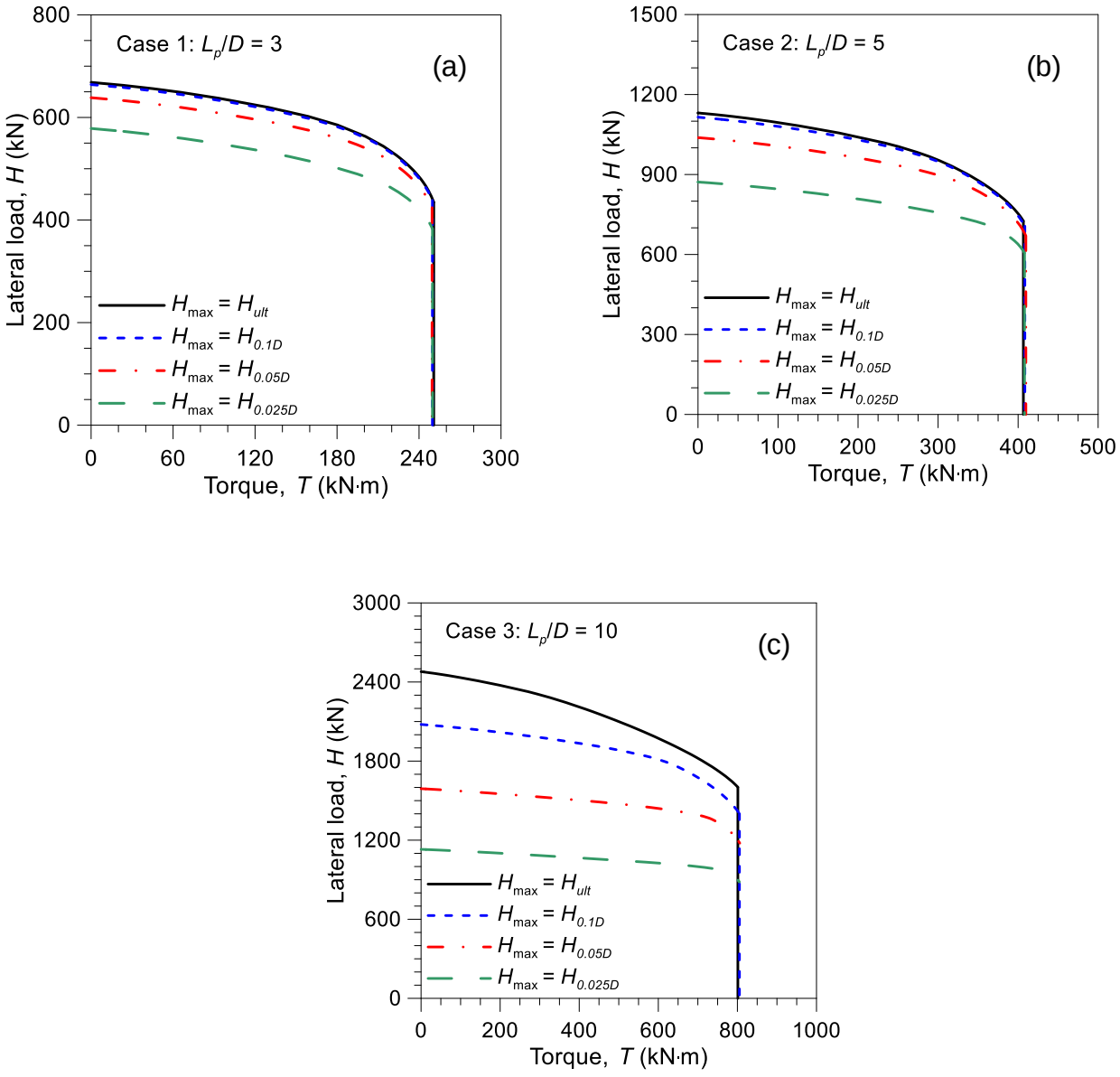

Figure 2.7. To illustrate how the charts in Figure 2.9 can be used for design, let us assume that the ultimate capacity criterion for lateral loading is defined as a load corresponding to a foundation head deflection of 10% of foundation diameter (H_{max} = $H_{0.1D}$). In the absence of a torsional loading (T/H = 0), 100% of H_{max} can be used as an ultimate lateral capacity. However, if the foundation is to be subjected to a simultaneous loading of a torque and a lateral load with a ratio T/H of 0.5 m (say, T = 250 kN-m and H = 500 kN), then the charts Figure 2.9 suggest that the full lateral capacity cannot be used and should be reduced to 70~73% of H_{max}. Similarly, for the ultimate capacity criterion of H_{max} = $H_{0.025D}$, the lateral capacity needs to be reduced to 79~92% of H_{max} for T/H = 0.5 m, depending on L_p/D. The greatest reduction of lateral capacity observed from the FEA was about 63% with a T/H of 0.58 m for L_p/D = 5 (refer to Figure 2.9b). Whether H/H_{max} continues to decrease beyond the range of T/H considered in this study is unknown at this time and warrants further investigation. Typical ranges of T/H for various transportation infrastructures will also need to be examined in future studies.

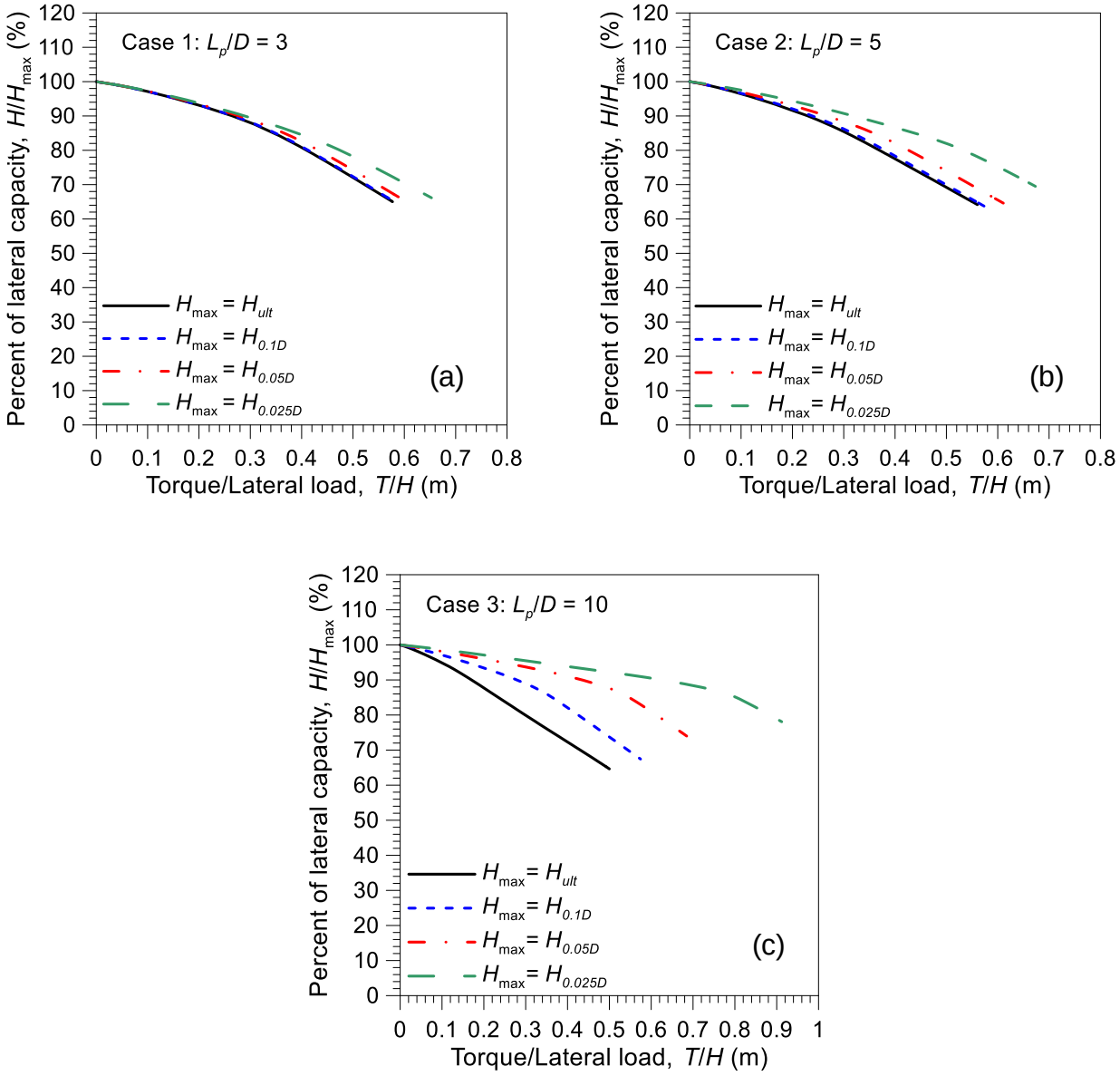

Figure 2.9 Lateral capacity reduction versus torque-to-lateral load ratio: (a) L_p/D = 3, (b) L_p/D = 5, and (c) L_p/D = 10

2.3.3 Failure mechanisms

To observe failure mechanisms of foundations subjected to combined lateral and torsional loads, the contour plots of maximum principal plastic strains obtained for the drilled shaft with L_p/D = 3 are presented, as a representative case, in Figure 2.10 for

various loading levels. The plastic zone is very small at lower loading levels but becomes greater as the lateral load increases. When an ultimate lateral load is applied, much higher levels of plastic strains are observed near the foundation head and base than the middle portion of the foundation (refer to the figure at H_{ult} in Figure 2.10a). Upon additional torsional loading, the plastic zone propagates along the foundation and the entire shaft is subjected to high plastic strain levels (refer to the figure at H_{ult}-T_{ult} in Figure 2.10a). Furthermore, the thickness of plastic zone becomes greater when the foundation is subjected an additional torsional loading (see the figure at H_{ult}-T_{ult} in Figure 2.10b).

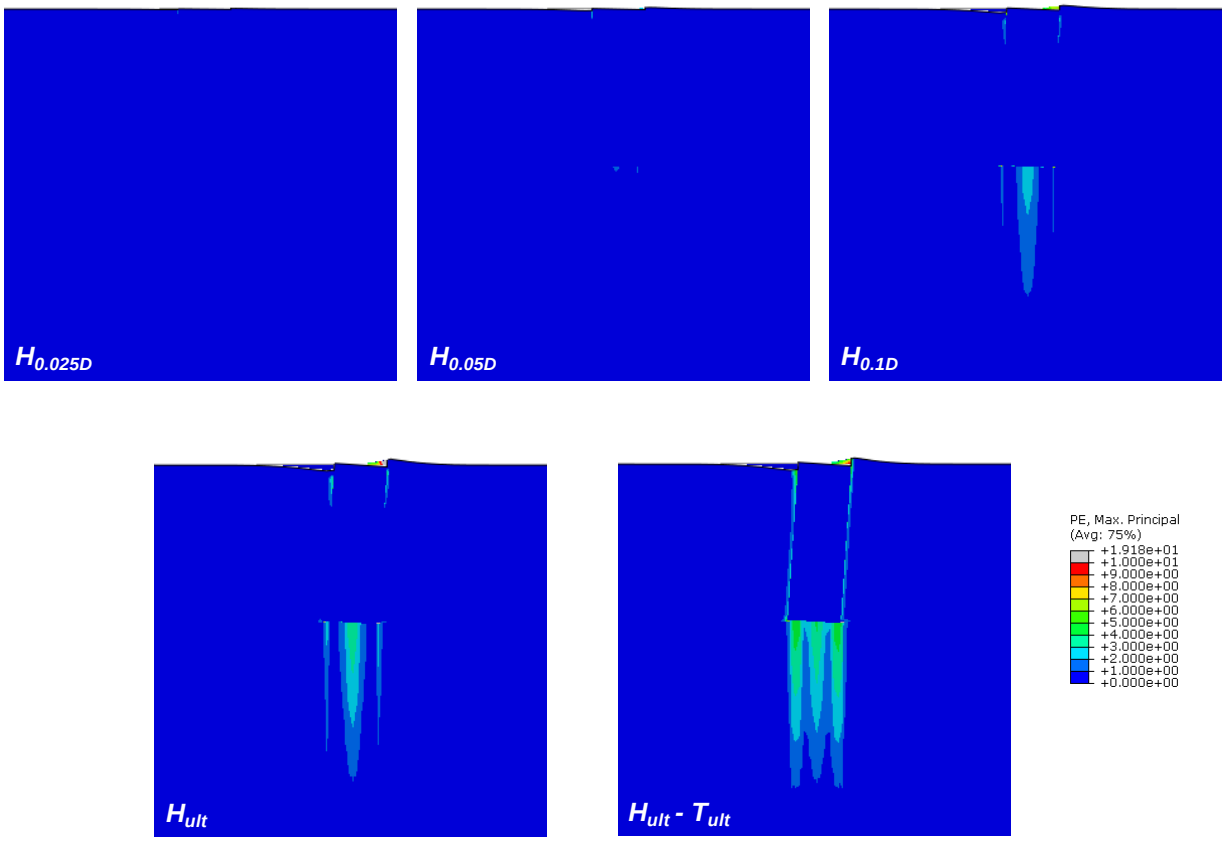

(a)

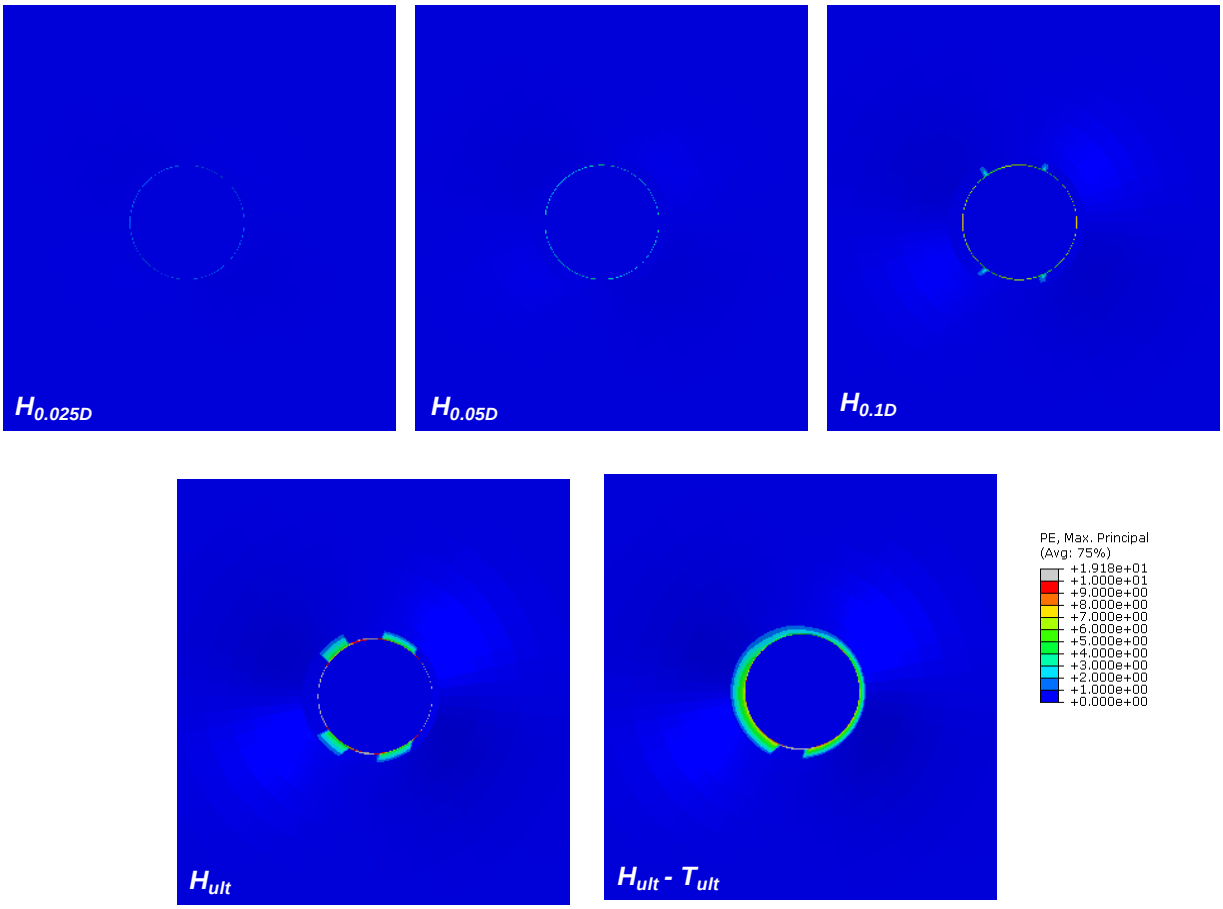

(b)

Figure 2.10 Contour plots of maximum principal plastic strains for L_p/D = 3: (a) front view and (b) top view

CHAPTER 3. ANALYTICAL MODELLING

3.1 Introduction

As seen in CHAPTER 2, FEA successfully captures the effect of combined loading of a torque and a lateral on the behavior of circular foundations. However, it requires extensive computational efforts to determine failure envelopes and is often beyond the reach of ordinary engineers who may not be well versed in FEA. This chapter presents our efforts to develop an easy-to-use-yet-mathematically-rigorous analysis tool through analytical modelling of a circular foundation subjected to concurrent application of lateral and torsional loads.

3.2 Mathematical formulation

3.2.1 Problem definition and basic assumptions

We consider a cylindrical foundation of length L_p and circular cross section of diameter D (=$2r_p$). The foundation, which is under a lateral load H and a torque T, is embedded in a total of N horizontal soil layers. The foundation itself crosses m layers, while $N - m$ layers exist below the base of the foundation. All soil layers extend to infinity in the radial direction, and the bottom (N^{th}) layer extends to infinity downward in the vertical direction. As shown in Figure 3.1, $z_{H,i}$ denotes the vertical depth from the ground surface to the bottom of any layer i, which implies that the thickness of layer i is $z_{H,i} - z_{H,i\text{-}1}$ with $z_{H,0} = 0$ and $z_{H,N} = \infty$.

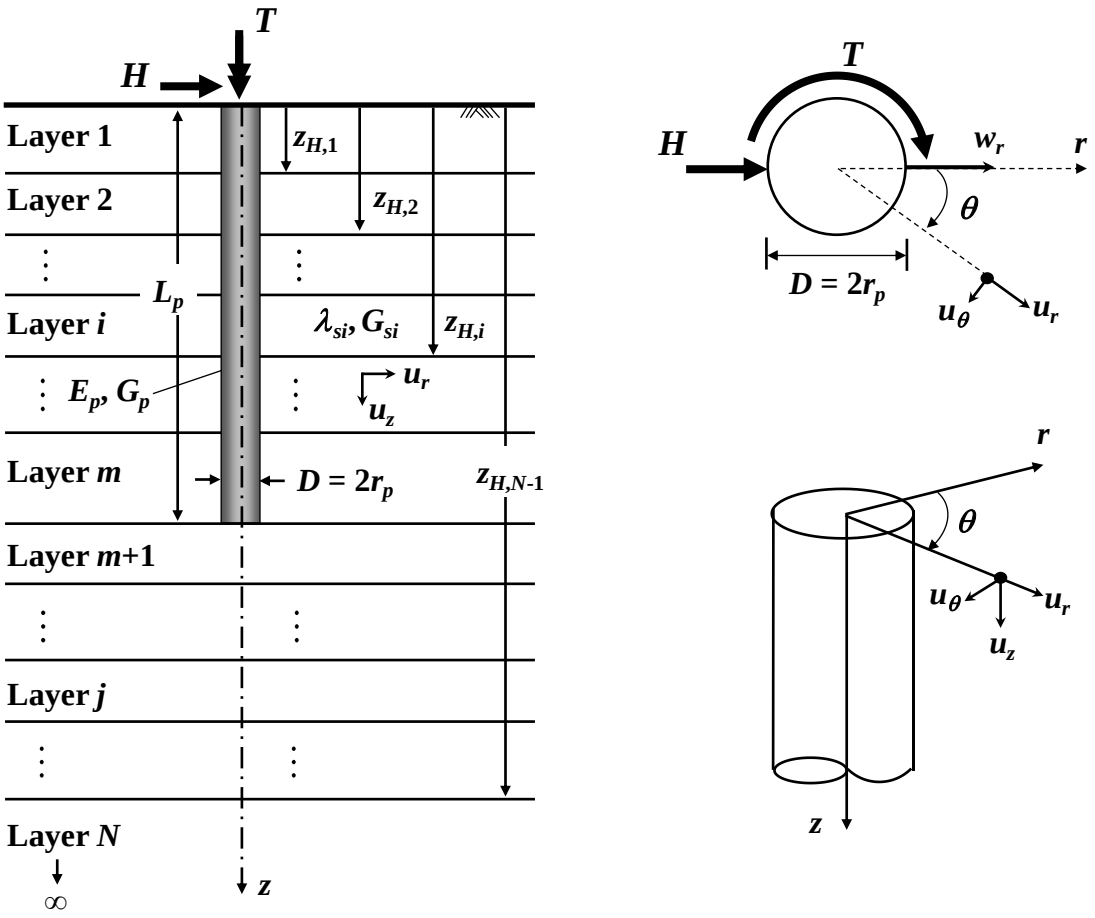

Figure 3.1 Geometry of the foundation-soil system

Since the problem is axisymmetric, we choose a system of cylindrical coordinates with the origin coinciding with the center of the foundation cross section at the foundation head and the z axis coinciding with the foundation axis (z is positive in the downward direction). The soil medium within each layer is assumed to be isotropic, homogeneous, and linear elastic, with elastic properties described by Lame's constants λ_{si} and G_{si}, which can be related to more recognizable $E_{si} - \nu_{si}$ pair of elastic constants: $\lambda_{si} = E_{si}\nu_{si}/[(1+\nu_{si})(1-2\nu_{si})]$ and $G_{si} = E_{si}/[2(1+\nu_{si})]$. The foundation is described as a linear elastic material with Young's modulus E_p and shear modulus G_p. It is also assumed that there is no slippage or separation between the foundation and the surrounding soil or between soil layers.

3.2.2 Soil displacements

The soil displacement fields at any point of soil medium are assumed to be a product of separable variables, as done by many researchers (Vlasov and Leont'ev 1966; Vallabhan and Mustafa 1996; Basu et al. 2009; Seo et al. 2009; Salgado et al. 2013), as follows:

$$u_r(r,\theta,z) = [w_r(z)\cos\theta]\phi_r(r) \tag{3.1}$$

$$u_\theta(r,\theta,z) = [-w_r(z)\sin\theta + w_\theta(z)]\phi_\theta(r) = [-w_r(z)\sin\theta + r_p\psi_p(z)]\phi_\theta(r) \tag{3.2}$$

$$u_z(r,\theta,z) = 0 \tag{3.3}$$

where $u_r(r, \theta, z)$, $u_\theta(r, \theta, z)$, and $u_z(r, \theta, z)$ = lateral, tangential, and vertical soil displacements, respectively, at any point (r, θ, z) in the soil mass (refer to Figure 3.1); $w_r(z)$ = lateral displacement at the foundation-soil interface as a function of depth z; $w_\theta(z)$ = tangential displacement at the foundation-soil interface as a function of depth z; $\psi_p(z)$ = angle of twist of the foundation cross section ($\psi_p = w_\theta/r_p$) varying with depth z; and $\phi_r(r)$ and $\phi_\theta(r)$ = dimensionless functions varying along the radial distance r; these ϕ functions are shape functions that describe the decreases in the soil displacements with increasing radial distance from the foundation axis. The ϕ functions are equal to one at the foundation-soil interface (*i.e.*, to $r = r_p$), and this ensures proper foundation-soil contact. Furthermore, the ϕ functions are zero at $r = \infty$ because the soil displacements must vanish at infinite horizontal distances from the foundation. Eq. (3.2) clearly states that the tangential soil displacement is influenced not only by the tangential displacement of the foundation due to the applied torque but also by the lateral displacement of the foundation caused by the lateral load. Eq. (3.3) assumes that the vertical displacement of the soil caused by the lateral and torsional loads is negligible.

3.2.3 Stress-strain-displacement relationships

The stress-strain relationship in an isotropic and elastic soil medium is expressed as follows:

$$\begin{bmatrix} \sigma_{rr} \\ \sigma_{\theta\theta} \\ \sigma_{zz} \\ \tau_{r\theta} \\ \tau_{rz} \\ \tau_{\theta z} \end{bmatrix} = \begin{bmatrix} \lambda_s + 2G_s & \lambda_s & \lambda_s & 0 & 0 & 0 \\ \lambda_s & \lambda_s + 2G_s & \lambda_s & 0 & 0 & 0 \\ \lambda_s & \lambda_s & \lambda_s + 2G_s & 0 & 0 & 0 \\ 0 & 0 & 0 & G_s & 0 & 0 \\ 0 & 0 & 0 & 0 & G_s & 0 \\ 0 & 0 & 0 & 0 & 0 & G_s \end{bmatrix} \begin{bmatrix} \varepsilon_{rr} \\ \varepsilon_{\theta\theta} \\ \varepsilon_{zz} \\ \gamma_{r\theta} \\ \gamma_{rz} \\ \gamma_{\theta z} \end{bmatrix} \tag{3.4}$$

where σ_{rr}, $\sigma_{\theta\theta}$, σ_{zz} = normal stresses; $\tau_{r\theta}$, τ_{rz}, $\tau_{\theta z}$ = shear stresses; ε_{rr}, $\varepsilon_{\theta\theta}$, ε_{zz} = normal strains; $\gamma_{r\theta}$, γ_{rz}, $\gamma_{\theta z}$ = shear strains.

With the assumed displacement field given in Eqs. (3.1) through (3.3), the strain-displacement relationship is given by:

$$\begin{bmatrix} \varepsilon_{rr} \\ \varepsilon_{\theta\theta} \\ \varepsilon_{zz} \\ \gamma_{r\theta} \\ \gamma_{rz} \\ \gamma_{\theta z} \end{bmatrix} = \begin{bmatrix} -\dfrac{\partial u_r}{\partial r} \\ -\dfrac{u_r}{r} - \dfrac{1}{r}\dfrac{\partial u_\theta}{\partial \theta} \\ -\dfrac{\partial u_z}{\partial z} \\ -\dfrac{1}{r}\dfrac{\partial u_r}{\partial \theta} - \dfrac{\partial u_\theta}{\partial r} + \dfrac{u_\theta}{r} \\ -\dfrac{\partial u_z}{\partial r} - \dfrac{\partial u_r}{\partial z} \\ -\dfrac{1}{r}\dfrac{\partial u_z}{\partial \theta} - \dfrac{\partial u_\theta}{\partial z} \end{bmatrix} = \begin{bmatrix} -w_r \dfrac{d\phi_r}{dr}\cos\theta \\ \dfrac{w_r \cos\theta}{r}(\phi_\theta - \phi_r) \\ 0 \\ w_r \dfrac{\phi_r}{r}\sin\theta + (w_r \sin\theta - r_p \psi_p)\left(\dfrac{d\phi_\theta}{dr} - \dfrac{\phi_\theta}{r}\right) \\ -\dfrac{dw_r}{dz}\phi_r \cos\theta \\ \left(\dfrac{dw_r}{dz}\sin\theta - r_p \dfrac{d\psi_p}{dz}\right)\phi_\theta \end{bmatrix} \tag{3.5}$$

3.2.4 Potential energy

The total potential energy Π of the foundation-soil system, including both internal and external potential energies, is given by.

$$\prod = U_{foundation} + U_{soil} - U_{external} \tag{3.6}$$

where $U_{foundation}$ = strain energy in the foundation, U_{soil} = strain energy in the soil, and $U_{external}$ = work done by external loads.

The strain energy stored in the foundation due to the bending and torsion is obtained as follows:

$$U_{foundation} = \frac{E_p I_p}{2} \int_0^{L_p} \left(\frac{d^2 w_r}{dz^2} \right)^2 dz + \frac{G_p J_p}{2} \int_0^{L_p} \left(\frac{d^2 \psi_p}{dz^2} \right)^2 dz \tag{3.7}$$

where I_p = moment of inertia of the foundation cross section (= $\pi r_p^4/4$) and J_p = polar moment of inertia of foundation cross section (= $\pi r_p^4/2$). Similarly, the strain energy in the soil is obtained by integrating the strain energy density of the soil (= $\frac{1}{2}\sigma_{pq}\varepsilon_{pq}$ where σ_{pq} and ε_{pq} are the stress and strain tensors in the soil, respectively) over the soil volume as follows:

$$\begin{aligned} U_{soil} = \frac{1}{2} \int_0^{\infty} \int_{r_p}^{\infty} \int_0^{2\pi} \Bigg[& \left(\lambda_s + 2G_s\right) \left(w_r \frac{d\phi_r}{dr} \cos\theta \right)^2 + \left(\lambda_s + 2G_s\right) \left\{ \frac{w_r \cos\theta}{r} (\phi_\theta - \phi_r) \right\}^2 \\ & - 2\lambda_s w_r^2 \frac{d\phi_r}{dr} \left(\frac{\phi_\theta - \phi_r}{r} \right) \cos^2\theta + G_s \left\{ w_r \frac{\phi_r}{r} \sin\theta + (w_r \sin\theta - r_p \psi_p) \left(\frac{d\phi_\theta}{dr} - \frac{\phi_\theta}{r} \right) \right\}^2 \\ & + G_s \left(\frac{dw_r}{dz} \phi_r \cos\theta \right)^2 + G_s \left\{ \left(\frac{dw_r}{dz} \sin\theta - r_p \frac{d\psi_p}{dz} \right) \phi_\theta \right\}^2 \Bigg] r d\theta dr dz \\ & + \frac{1}{2} \int_{L_p}^{\infty} \int_0^{r_p} \int_0^{2\pi} \left[G_s \left(\frac{r_p \psi_p}{r} \right)^2 + G_s \left(\frac{dw_r}{dz} \cos\theta \right)^2 + G_s \left(\frac{dw_r}{dz} \sin\theta - r_p \frac{d\psi_p}{dz} \right)^2 \right] r d\theta dr dz \end{aligned} \tag{3.8}$$

For the multilayered system as shown in Figure 3.1, Eq. (3.8) can be rewritten with properties of each soil layer:

$$
\begin{aligned}
U_{soil} = \sum_{i=1}^{N} \frac{\pi}{2} \int_{z_{H,i-1}}^{z_{H,i}} \int_{r_p}^{\infty} \Bigg[& \left(\lambda_{si} + 2G_{si}\right) w_{ri}^2 \left(\frac{d\phi_r}{dr} \right)^2 + \left(\lambda_{si} + 2G_{si}\right) w_{ri}^2 \left(\frac{\phi_\theta - \phi_r}{r} \right)^2 \\
& - 2\lambda_{si} w_{ri}^2 \frac{d\phi_r}{dr} \left(\frac{\phi_\theta - \phi_r}{r} \right) + G_{si} \left(\frac{w_{ri}\phi_r}{r} \right)^2 + G_{si} w_{ri}^2 \left(\frac{d\phi_\theta}{dr} - \frac{\phi_\theta}{r} \right)^2 + 2r_p^2 G_{si} \psi_{pi}^2 \left(\frac{d\phi_\theta}{dr} - \frac{\phi_\theta}{r} \right)^2 \\
& + 2G_{si} w_{ri}^2 \frac{\phi_r}{r} \left(\frac{d\phi_\theta}{dr} - \frac{\phi_\theta}{r} \right) + G_{si} \left(\frac{dw_{ri}}{dz} \right)^2 \left(\phi_r^2 + \phi_\theta^2 \right) + 2G_{si} r_p^2 \left(\frac{d\psi_{pi}}{dz} \right)^2 \phi_\theta^2 \Bigg] r dr dz \\
& + \sum_{i=m+1}^{N} \frac{\pi}{2} \int_{z_{H,i-1}}^{z_{H,i}} \int_{0}^{r_p} \left[2G_{si} \left(\frac{r_p \psi_{pi}}{r} \right)^2 + 2G_{si} \left(\frac{dw_{ri}}{dz} \right)^2 + 2G_{si} r_p^2 \left(\frac{d\psi_{pi}}{dz} \right)^2 \right] r dr dz
\end{aligned}
\tag{3.9}
$$

where w_{ri} and ψ_{pi} are the functions $w_r(z)$ and $\psi_p(z)$ within the i^{th} layer.

The work done by external loads is given by:

$$
U_{external} = H\, w_r\big|_{z=0} + T\, \psi_p\big|_{z=0} \tag{3.10}
$$

3.2.5 Principle of minimum potential energy

The principle of minimum potential energy states that a conservative system attains its equilibrium formation when its total potential energy is at a minimum (i.e. setting the first variation of the potential energy $\delta\Pi$ equal to zero, where δ is a variational operator). Applying $\delta\Pi = 0$ to Eq. (3.6) yields many terms that contain the first variations δw_r, $\delta\phi_r$, $\delta\psi_p$, and $\delta\phi_\theta$, and we obtain the following form of the equation by collecting and rearranging the terms:

$$
A(w_r)\delta w_r + B(\phi_r)\delta\phi_r + C(\psi_p)\delta\psi_p + D(\phi_\theta)\delta\phi_\theta = 0 \tag{3.11}
$$

Because the functions w_r, ϕ_r, ψ_p, and ϕ_θ in Eq. (3.11) are not known *a priori*, their variations are not zero according to the variational principle. Furthermore, since these functions are independent one another, Eq. (3.11) is satisfied if and only if their coefficients $A(w_r)$, $B(\phi_r)$, $C(\psi_p)$, and $D(\phi_\theta)$ are all zero. The equilibrium configuration of the foundation-soil system is obtained when these expressions [$A(w_r) = 0$, $B(\phi_r) = 0$, $C(\psi_p) = 0$, and $D(\phi_\theta) = 0$] are solved, which represent the governing differential equations of the functions $w_r(z)$, $\phi_r(r)$, $\psi_p(z)$, and $\phi_\theta(r)$.

3.2.6 Governing differential equation for lateral displacement function w_r

The governing differential equation for the lateral displacement function $w_{ri}(z)$ in any layer i is obtained by equating the coefficients of δw_{ri} to zero. Two sub-domains are considered for the function $w_{ri}(z)$: within the foundation length ($0 \le z \le L_p$) and beneath the foundation ($L_p < z < \infty$).

For the domain within the foundation length ($0 \le z \le L_p$), the governing differential equation for the function $w_{ri}(z)$ is given as

$$E_p I_p \frac{d^4 w_{ri}}{dz^4} - 2t_{ri} \frac{d^2 w_{ri}}{dz^2} + k_{ri} w_{ri} = 0 \tag{3.12}$$

and, the differential equation for the domain beneath the foundation ($L_p < z < \infty$) is given as

$$-2t_{ri} \frac{d^2 w_{ri}}{dz^2} + k_{ri} w_{ri} = 0 \tag{3.13}$$

where

$$t_{ri} = \begin{cases} \dfrac{\pi G_{si}}{2} \displaystyle\int_{r_p}^{\infty} (\phi_r^{\,2} + \phi_\theta^{\,2}) r dr; \;\; i = 1, 2, \cdots, m \\ \dfrac{\pi G_{si}}{2} \left[\displaystyle\int_{r_p}^{\infty} (\phi_r^{\,2} + \phi_\theta^{\,2}) r dr + r_p^2 \right]; \;\; i = m+1, \cdots, N \end{cases} \tag{3.14}$$

$$k_{ri}=\pi\left[\left(\lambda_{si}+2G_{si}\right)\int_{r_p}^{\infty}\left(\frac{d\phi_r}{dr}\right)^2 rdr+G_{si}\int_{r_p}^{\infty}\left(\frac{d\phi_\theta}{dr}\right)^2 rdr+2\lambda_{si}\int_{r_p}^{\infty}\left(\phi_r-\phi_\theta\right)\frac{d\phi_r}{dr}dr\right.$$
$$\left.+2G_{si}\int_{r_p}^{\infty}\left(\phi_r-\phi_\theta\right)\frac{d\phi_\theta}{dr}dr+\left(\lambda_{si}+3G_{si}\right)\int_{r_p}^{\infty}\frac{1}{r}\left(\phi_r-\phi_\theta\right)^2 dr\right];\quad i=1,2,\cdots,N \tag{3.15}$$

Note that the index *i* for the domain within the foundation length ($0 \le z \le L_p$) ranges from 1 to *m* and, for the domain beneath the foundation base it ranges from *m*+1 to *N* (see Figure 3.1). Because Eq. (3.12) is 4th order differential equation and there are *m* layers within the foundation, a total of 4*m* boundary conditions are needed to solve Eq. (3.12). First, four boundary conditions are obtained at the foundation head and base as follows:

$$E_p I_p\frac{d^3 w_{r1}(0)}{dz^3}-2t_{r1}\frac{dw_{r1}(0)}{dz}=H \tag{3.16}$$
(shear force at foundation head = applied lateral load)

$$E_p I_p\frac{d^2 w_{r1}(0)}{dz^2}=0 \text{ (bending moment at foundation head = 0)} \tag{3.17}$$

$$E_p I_p\frac{d^3 w_{rm}(L_p)}{dz^3}-2t_{rm}\frac{dw_{rm}(L_p)}{dz}=-2t_{r(m+1)}\frac{dw_{r(m+1)}(L_p)}{dz} \tag{3.18}$$
(continuity of shear force at foundation base)

$$E_p I_p\frac{d^2 w_{rm}(L_p)}{dz^2}=0 \text{ (bending moment at foundation base = 0)} \tag{3.19}$$

The remaining boundary conditions are then obtained from the continuity of variables at the interfaces within the foundation. These conditions yield 4*m* – 4 equations as follows because we have *m*–1 interfaces (*i* =1, 2, …, *m*–1):

$$w_{ri}(z_{H,i}) = w_{r(i+1)}(z_{H,i}) \text{ (continuity of foundation displacement)} \quad (3.20)$$

$$\frac{dw_{ri}(z_{H,i})}{dz} = \frac{dw_{r(i+1)}(z_{H,i})}{dz} \text{ (continuity of slope of foundation displacement)} \quad (3.21)$$

$$E_p I_p \frac{d^2 w_{ri}(z_{H,i})}{dz^2} = E_p I_p \frac{d^2 w_{r(i+1)}(z_{H,i})}{dz^2} \text{ (continuity of foundation bending moment)} \quad (3.22)$$

$$E_p I_p \frac{d^3 w_{ri}(z_{H,i})}{dz^3} - 2t_{ri} \frac{dw_{ri}(z_{H,i})}{dz} = E_p I_p \frac{d^3 w_{r(i+1)}(z_{H,i})}{dz^3} - 2t_{r(i+1)} \frac{dw_{r(i+1)}(z_{H,i})}{dz} \quad (3.23)$$

(continuity of shear force in foundation)

Similarly, Eq. (3.13) is 2nd order differential equation and there are $N - m$ layers beneath the foundation base; therefore, a total of $2(N - m)$ boundary conditions are needed to solve Eq. (3.13). Two boundary conditions are obtained at the foundation base and infinite depth as follows:

$$w_{rm}(L_p) = w_{r(m+1)}(L_p) \text{ (displacement continuity at foundation base)} \quad (3.24)$$

$$w_{rN}(\infty) = 0 \text{ (zero displacement at infinite depth)} \quad (3.25)$$

The remaining $2(N - m) - 2$ boundary conditions are obtained from the continuity of variables at the interfaces between the two neighboring soil layers beneath the foundation base ($i = m+1, \ldots, N-1$) as follows:

$$w_{ri}(z_{H,i}) = w_{r(i+1)}(z_{H,i}) \text{ (continuity of soil displacement)} \quad (3.26)$$

$$2t_{ri} \frac{dw_{ri}(z_{H,i})}{dz} = 2t_{r(i+1)} \frac{dw_{r(i+1)}(z_{H,i})}{dz} \text{ (continuity of shear force in soil)} \quad (3.27)$$

3.2.7 Governing differential equation for angle of twist function ψ_p

The governing differential equation for the angle of twist function $\psi_{pi}(z)$ in any layer *i* is obtained by equating the coefficients of $\delta\psi_{pi}$ to zero. Two sub-domains exist for the function $\psi_{pi}(z)$: within the foundation length ($0 \le z \le L_p$) and beneath the foundation ($L_p < z < \infty$).

For the domain within the foundation length ($0 \le z \le L_p$), the governing differential equation for the function $\psi_{pi}(z)$ is given as

$$-(G_p J_p + 2t_{\theta i})\frac{d^2\psi_{pi}}{dz^2} + k_{\theta i}\psi_{pi} = 0 \tag{3.28}$$

and, the differential equation for the domain beneath the foundation ($L_p < z < \infty$) is given as

$$-2t_{\theta i}\frac{d^2\psi_{pi}}{dz^2} + k_{\theta i}\psi_{pi} = 0 \tag{3.29}$$

where

$$t_{\theta i} = \begin{cases} \pi r_p^2 G_{si}\int_{r_p}^{\infty}\phi_\theta{}^2 r dr; \ i = 1,2,\cdots,m \\ \pi r_p^2 G_{si}\left(\frac{r_p^2}{2} + \int_{r_p}^{\infty}\phi_\theta{}^2 r dr\right); \ i = m+1,\cdots,N \end{cases} \tag{3.30}$$

$$k_{\theta i} = \begin{cases} 2\pi r_p^2 G_{si}\int_{r_p}^{\infty}\left(\frac{d\phi_\theta}{dr} - \frac{\phi_\theta}{r}\right)^2 r dr; \ i = 1,2,\cdots,m \\ 2\pi r_p^2 G_{si}\left[\ln(r_p) - \lim_{\varepsilon\to 0}\{\ln(\varepsilon)\} + \int_{r_p}^{\infty}\left(\frac{d\phi_\theta}{dr} - \frac{\phi_\theta}{r}\right)^2 r dr\right]; \ i = m+1,\cdots,N \end{cases} \tag{3.31}$$

Note that in Eq. (3.31) $k_{\theta i}$ beneath the foundation base is not defined at $r = 0$ because ln(0) is undefined. To avoid such a numerical issue, the lower limit of integration was changed from $r = 0$ to $r = \varepsilon$ where ε is taken as a sufficiently small positive number (ε = 0.001 m is used in this study).

Because Eq. (3.28) is 2nd order differential equation and there are m layers within the foundation, a total of 2m boundary conditions are needed to solve Eq. (3.28). First, two boundary conditions are obtained at the foundation head and base as follows:

$$-(G_p J_p + 2t_{\theta 1})\frac{d\psi_{p1}(0)}{dz} = T \quad \text{(torque at foundation head = applied torque)} \tag{3.32}$$

$$-(G_p J_p + 2t_{\theta m})\frac{d\psi_{pm}(L_p)}{dz} = -2t_{\theta(m+1)}\frac{d\psi_{p(m+1)}(L_p)}{dz} \tag{3.33}$$

(continuity of torque at foundation base)

The remaining 2m – 2 boundary conditions are then obtained from the continuity requirements at the interfaces within the foundation (i =1, 2, …, m-1) as follows:

$$\psi_{pi}(z_{H,i}) = \psi_{p(i+1)}(z_{H,i}) \quad \text{(continuity of angle of twist of foundation)} \tag{3.34}$$

$$-(G_p J_p + 2t_{\theta i})\frac{d\psi_{pi}(z_{H,i})}{dz} = (G_p J_p + 2t_{\theta(i+1)})\frac{d\psi_{p(i+1)}(z_{H,i})}{dz} \tag{3.35}$$

(continuity of torque in foundation)

Similarly, a total of 2(N – m) boundary conditions are needed to solve Eq. (3.29). Two boundary conditions are obtained at the foundation base and infinite depth as follows:

$$\psi_{pm}(L_p) = \psi_{p(m+1)}(L_p) \quad \text{(continuity of angle of twist at foundation base)} \tag{3.36}$$

$$\psi_{pN}(\infty) = 0 \text{ (zero angle of twist at infinite depth)} \tag{3.37}$$

The remaining 2(N – m) – 2 boundary conditions are obtained from the continuity requirements at the interfaces between the two neighboring soil layers beneath the foundation base (i = m+1, …, N-1) as follows:

$$\psi_{pi}(z_{H,i}) = \psi_{p(i+1)}(z_{H,i}) \text{ (continuity of angle of twist of soil column)} \tag{3.38}$$

$$-2t_{\theta i}\frac{d\psi_{pi}(z_{H,i})}{dz} = -2t_{\theta(i+1)}\frac{d\psi_{p(i+1)}(z_{H,i})}{dz} \text{ (continuity of torque in soil column)} \tag{3.39}$$

3.2.8 Governing differential equation for lateral displacement decay function ϕ_r in soil

The governing differential equation for the lateral displacement decay function $\phi_r(r)$ in the soil is obtained by equating the coefficients of $\delta\phi_r$ to zero and given as

$$\frac{d^2\phi_r}{dr^2} + \frac{1}{r}\frac{d\phi_r}{dr} - \left[\left(\frac{\gamma_{rs1}}{r}\right)^2 + \left(\frac{\gamma_{rs2}}{r_p}\right)^2\right]\phi_r = -\left(\frac{\gamma_{rs1}}{r}\right)^2\phi_\theta + \frac{\gamma_{rs3}^2}{r}\frac{d\phi_\theta}{dr} \tag{3.40}$$

where

$$\gamma_{rs1} = \sqrt{\frac{\sum_{i=1}^{N}\left(\lambda_{si} + 3G_{si}\right)\int_{z_{H,i-1}}^{z_{H,i}} w_{ri}^{\,2}\,dz}{\sum_{i=1}^{N}\left(\lambda_{si} + 2G_{si}\right)\int_{z_{H,i-1}}^{z_{H,i}} w_{ri}^{\,2}\,dz}} \tag{3.41}$$

$$\gamma_{rs2} = r_p\sqrt{\frac{\sum_{i=1}^{N} G_{si}\int_{z_{H,i-1}}^{z_{H,i}}\left(\frac{dw_{ri}}{dz}\right)^2 dz}{\sum_{i=1}^{N}\left(\lambda_{si} + 2G_{si}\right)\int_{z_{H,i-1}}^{z_{H,i}} w_{ri}^{\,2}\,dz}} \tag{3.42}$$

$$\gamma_{rs3}=\sqrt{\frac{\sum_{i=1}^{N}G_{si}\int_{z_{H,i-1}}^{z_{H,i}}w_{ri}{}^{2}dz+\sum_{i=1}^{N}\lambda_{si}\int_{z_{H,i-1}}^{z_{H,i}}w_{ri}{}^{2}dz}{\sum_{i=1}^{N}\left(\lambda_{si}+2G_{si}\right)\int_{z_{H,i-1}}^{z_{H,i}}w_{ri}{}^{2}dz}} \tag{3.43}$$

Boundary conditions for Eq. (3.40) are $\phi_r(r_p) = 1$ and $\phi_r(\infty) = 0$.

3.2.9 Governing differential equation for lateral displacement decay function ϕ_θ in soil

The governing differential equation for the tangential displacement decay function $\phi_\theta(r)$ in the soil is obtained by equating the coefficients of $\delta\phi_\theta$ to zero and given as

$$\frac{d^2\phi_\theta}{dr^2}+\frac{1}{r}\frac{d\phi_\theta}{dr}-\left[\left(\frac{\gamma_{\theta s1}}{r}\right)^2+\left(\frac{\gamma_{\theta s2}}{r_p}\right)^2\right]\phi_\theta=-\left(\frac{\gamma_{\theta s3}}{r}\right)^2\phi_r-\frac{\gamma_{\theta s4}^2}{r}\frac{d\phi_r}{dr} \tag{3.44}$$

where

$$\gamma_{\theta s1}=\sqrt{\frac{\sum_{i=1}^{N}\left(\lambda_{si}+3G_{si}\right)\int_{z_{H,i-1}}^{z_{H,i}}w_{ri}{}^{2}dz+\sum_{i=1}^{N}2\pi r_pG_{si}\int_{z_{H,i-1}}^{z_{H,i}}\psi_{pi}^{2}dz}{\sum_{i=1}^{N}G_{si}\int_{z_{H,i-1}}^{z_{H,i}}w_{ri}{}^{2}dz+\sum_{i=1}^{N}2\pi r_pG_{si}\int_{z_{H,i-1}}^{z_{H,i}}\psi_{pi}^{2}dz}} \tag{3.45}$$

$$\gamma_{\theta s2}=r_p\sqrt{\frac{\sum_{i=1}^{N}G_{si}\int_{z_{H,i-1}}^{z_{H,i}}\left(\frac{dw_{ri}}{dz}\right)^2dz+\sum_{i=1}^{N}2\pi r_p{}^{2}G_{si}\int_{z_{H,i-1}}^{z_{H,i}}\left(\frac{d\psi_{pi}}{dz}\right)^2dz}{\sum_{i=1}^{N}G_{si}\int_{z_{H,i-1}}^{z_{H,i}}w_{ri}{}^{2}dz+\sum_{i=1}^{N}2\pi r_pG_{si}\int_{z_{H,i-1}}^{z_{H,i}}\psi_{pi}^{2}dz}} \tag{3.46}$$

$$\gamma_{\theta s3} = \sqrt{\frac{\sum_{i=1}^{N}\left(\lambda_{si}+3G_{si}\right)\int_{z_{H,i-1}}^{z_{H,i}} w_{ri}{}^{2}dz}{\sum_{i=1}^{N}G_{si}\int_{z_{H,i-1}}^{z_{H,i}} w_{ri}{}^{2}dz+\sum_{i=1}^{N}2\pi r_{p}G_{si}\int_{z_{H,i-1}}^{z_{H,i}}\psi_{pi}^{2}dz}} \tag{3.47}$$

$$\gamma_{\theta s4} = \sqrt{\frac{\sum_{i=1}^{N}\left(\lambda_{si}+G_{si}\right)\int_{z_{H,i-1}}^{z_{H,i}} w_{ri}{}^{2}dz}{\sum_{i=1}^{N}G_{si}\int_{z_{H,i-1}}^{z_{H,i}} w_{ri}{}^{2}dz+\sum_{i=1}^{N}2\pi r_{p}G_{si}\int_{z_{H,i-1}}^{z_{H,i}}\psi_{pi}^{2}dz}} \tag{3.48}$$

Boundary conditions for Eq. (3.44) are $\phi_\theta(r_p) = 1$ and $\phi_\theta(\infty) = 0$. Note that Eqs. (3.40) and (3.44) contain both ϕ_r and ϕ_θ, suggesting that these functions are interdependent. A total of six differential equations represent the entire foundation-soil system under combined lateral and torsional loads, and they are summarized in Figure 3.2.

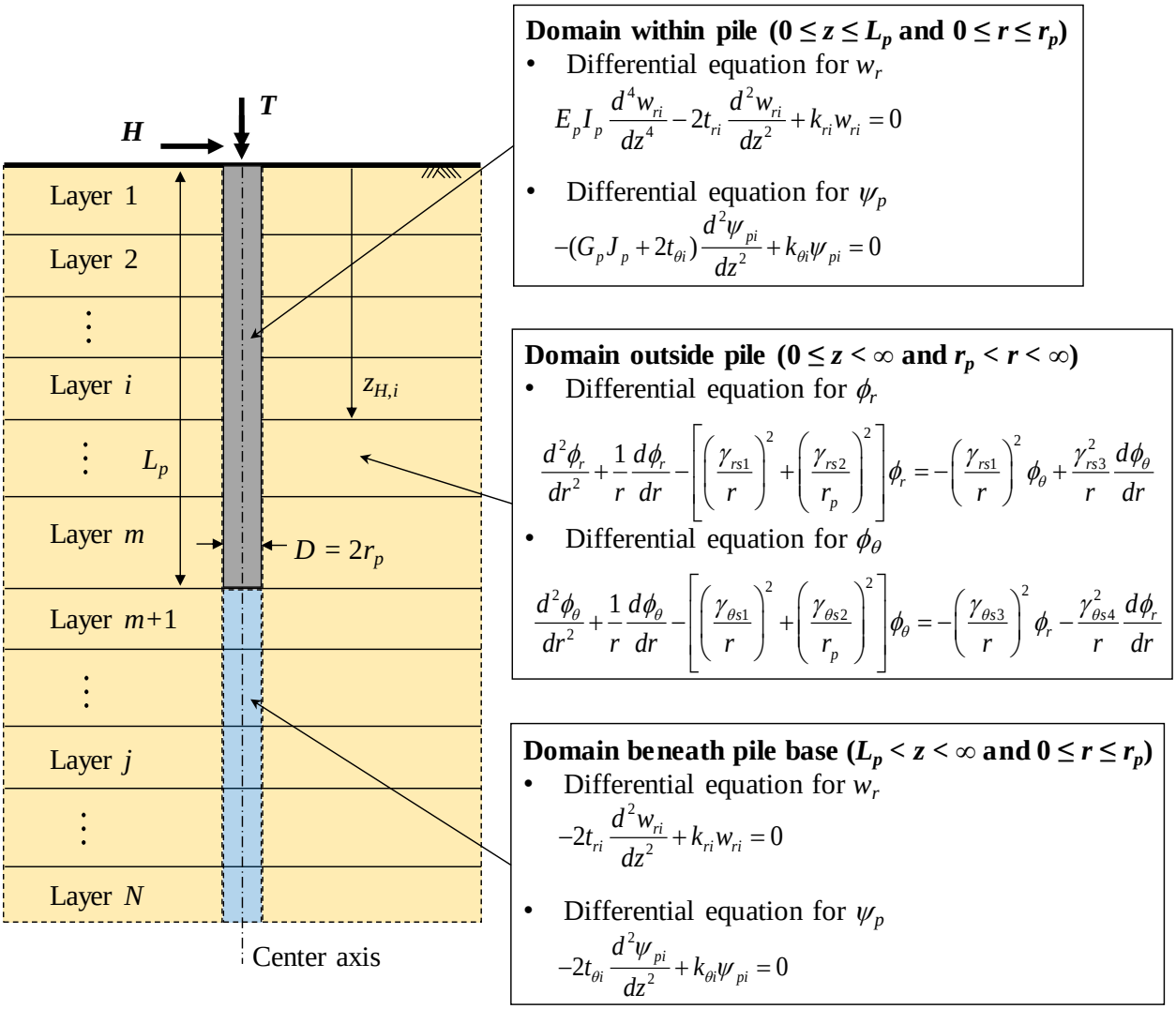

Figure 3.2 Differential equations in each sub-domain

3.2.10 Iterative solution scheme

Lateral displacement w_r and angle of twist ψ_p of the foundation and the soil column beneath the foundation are obtained by solving Eqs. (3.12), (3.13), (3.28), and (3.29) numerically using the finite difference method. To solve them, the soil resistance parameters t_{ri}, k_{ri}, $t_{\theta i}$ and $k_{\theta i}$ must be known, and these t and k parameters are functions of ϕ_r and ϕ_θ, as seen in Eqs. (3.14), (3.15), (3.30). However, to obtain ϕ_r and ϕ_θ by solving Eqs. (3.40) and (3.44), the parameters γ_{rs} and $\gamma_{\theta s}$ must be known *a priori*, but

they in turn depend on w_r and ψ_p [refer to Eqs. (3.40) through (3.48)]. Due to the interdependence of the soil and foundation differential equations, an iterative solution scheme is required in our analytical model.

The iterative solution scheme employed in this study begin by assuming initial values of γ_{rs} parameters (γ_{rs1}^{old}, γ_{rs2}^{old} and γ_{rs3}^{old}) and $\gamma_{\theta s}$ parameters ($\gamma_{\theta s1}^{old}$, $\gamma_{\theta s2}^{old}$, $\gamma_{\theta s3}^{old}$ and $\gamma_{\theta s4}^{old}$). Furthermore, due to interdependence of ϕ_r and ϕ_θ, we assume initial values of ϕ_θ that satisfies the boundary conditions [*i.e.*, $\phi_\theta(r_p) = 1$ and $\phi_\theta(\infty) = 0$]. With the assumed γ_{rs} parameters and ϕ_θ, the function ϕ_r is obtained by solving Eq. (3.40). Then, using the obtained ϕ_r and assumed $\gamma_{\theta s}$ parameters, new values of function ϕ_θ is calculated by solving Eq. (3.44). Because we now have solution to ϕ_r and ϕ_θ, the soil resistance parameters t_{ri}, k_{ri}, $t_{\theta i}$ and $k_{\theta i}$ are then calculated via numerical integration. With the soil resistance parameters t_{ri}, k_{ri}, $t_{\theta i}$ and $k_{\theta i}$ known, w_r and ψ_p are obtained by solving Eqs. (3.12), (3.13), (3.28), and (3.29). Then, new values of γ_{rs} parameters (γ_{rs1}^{new}, γ_{rs2}^{new} and γ_{rs3}^{new}) and $\gamma_{\theta s}$ parameters ($\gamma_{\theta s1}^{new}$, $\gamma_{\theta s2}^{new}$, $\gamma_{\theta s3}^{new}$ and $\gamma_{\theta s4}^{new}$) are calculated using the computed values of w_r and ψ_p and compared against the assumed initial values. If the differences are greater than the prescribed tolerance (a value of 10^{-5} was used in this study), iterations are continued with the calculated values of γ_{rs} and $\gamma_{\theta s}$ parameters taken as the new guess ($\gamma_{rs}^{old} = \gamma_{rs}^{new}$ and $\gamma_{\theta s}^{old} = \gamma_{\theta s}^{new}$) until the differences between old and new γ parameters from two successive iterations fall below the prescribed tolerance for all γ parameters. The iterative solution scheme is provided in the form of a flow chart in Figure 3.3.

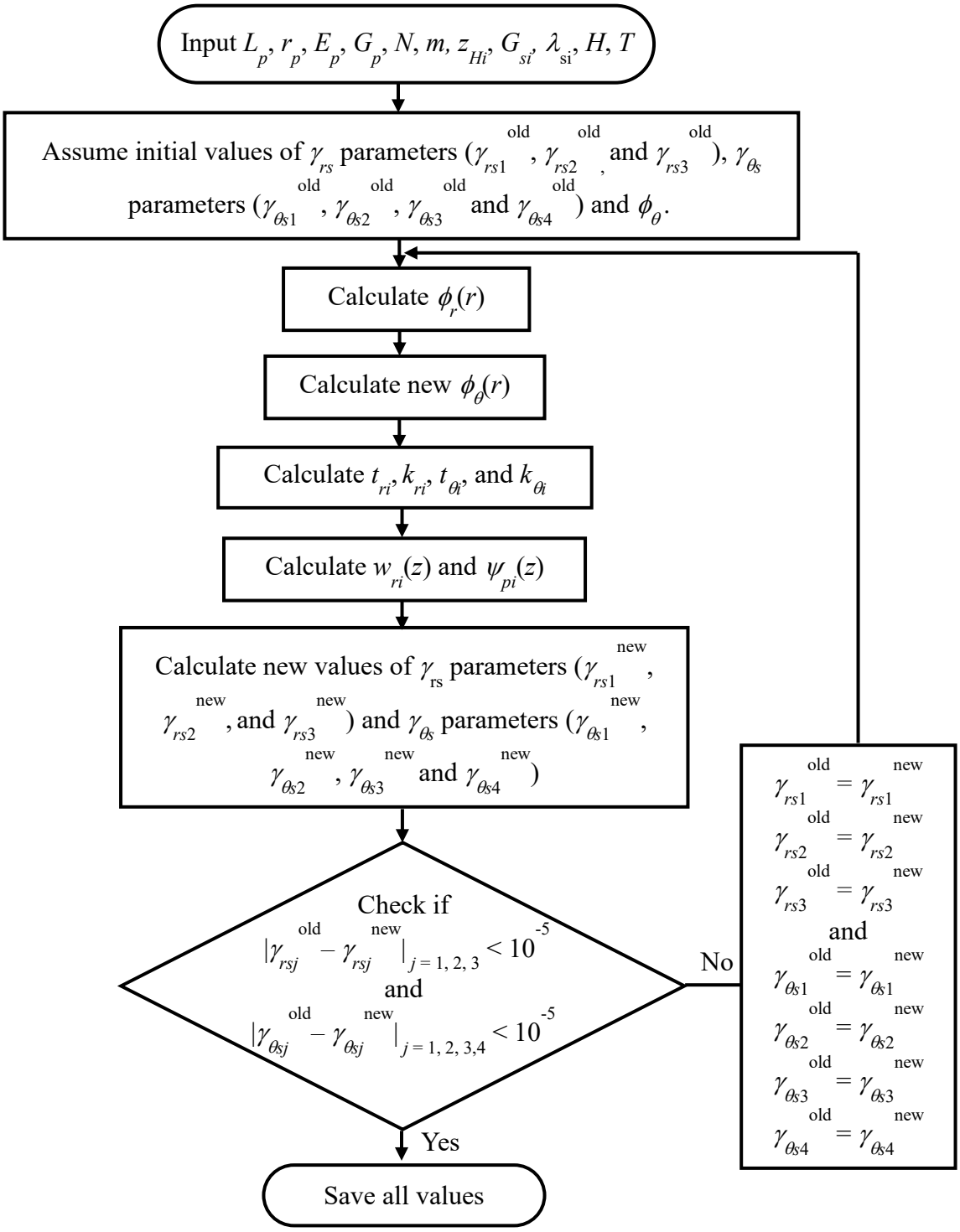

Figure 3.3 Flow chart for iterative solution scheme

3.3 Results and validations

Due to the absence of any previous analytical studies for a foundation under simultaneous loading of a lateral load and a torque, the validations are done for pure torsion and pure lateral load cases.

3.3.1 Lateral analysis

Basu et al. (2009) developed semi-analytical solutions for laterally loaded foundations in multilayered elastic soil using the variational principles and method of initial parameters. Our analysis model are derived from the same variational principles but with the displacement field resulted from *both* lateral deflection w_r and angle of twist ψ_p. Consequently, as seen in Eqs. (3.45) through (3.48), the γ factors associated with ϕ_θ become functions of both w_r and ψ_p. However, with the absence of the angle of twist ψ_p, the differential equations for w_r, ϕ_r, and ϕ_θ obtained from our study are simplified to the same differential equations derived in Basu et al.'s study. Therefore, when zero torque is applied in our analysis, the results from our study are expected to be the same as those from Basu et al.'s study. To verify this, we compare results from our analysis under zero torque against those from Basu et al.'s study for two example cases reported in their paper.

The first example considers a drilled shaft, 0.6 m in diameter and 15 m long, with Young's modulus E_p = 24 GPa, embedded in a four-layered soil profile. Properties of the four soil layers are as follows: E_{s1} = 20 MPa, ν_{s1} = 0.35, and $z_{H,1}$ = 2 m for Layer 1; E_{s2} = 35 MPa, ν_{s2} = 0.25, and $z_{H,2}$ = 5 m for Layer 2; E_{s3} = 50 MPa, ν_{s3} = 0.20, and $z_{H,3}$ = 8.3 m for Layer 3; and E_{s4} = 80 MPa and ν_{s4} = 0.15 for Layer 4 (Layer 4 extends from the bottom of the third layer to great depth). The applied lateral load H at the foundation head is 300 kN with zero torque (*i.e.*, T = 0).

The second example considers a drilled shaft, 1.7 m in diameter and 40 m long, with Young's modulus E_p = 25 GPa, embedded in a four-layered soil profile. The top three layers are located over 0-1.5 m, 1.5-5 m, and 5-13.5 m below the ground surface. The fourth layer extends from the bottom of the third layer to great depth. The elastic

constants of the four layers are as follows: E_{s1} = 20 MPa and ν_{s1} = 0.35 for Layer 1, E_{s2} = 25 MPa and ν_{s2} = 0.30 for Layer 2, E_{s3} = 40 MPa and ν_{s3} = 0.25 for Layer 3, and E_{s4} = 80 MPa and ν_{s4} = 0.20 for Layer 4. A lateral load of H = 3000 kN is applied at the foundation head with zero torque.

Profiles of lateral displacement along the shaft obtained from our analysis and the study by Basu et al. (2009) for the two examples are presented in Figure 3.4. As expected, they show excellent agreements for both examples. For the first example with D = 0.6 m and L_p = 15 m, we performed finite element analysis using ABAQUS for comparison purpose. Although our analysis yields slightly stiffer response than FEA (perhaps due to the assumption of zero vertical soil displacement made in our analysis), it is much more efficient than FEA, in addition to being faster, in terms of pre- and post-processing of the data due to its analytical nature.

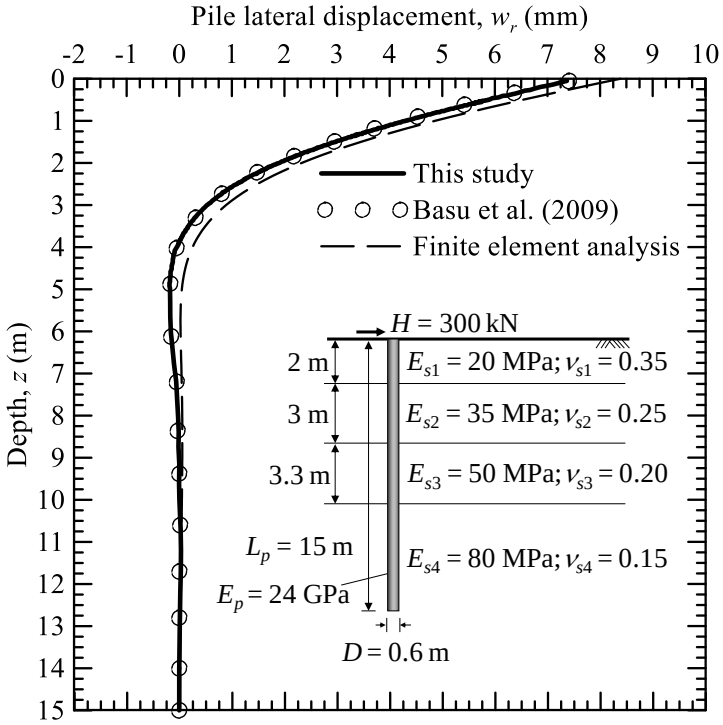

(a)

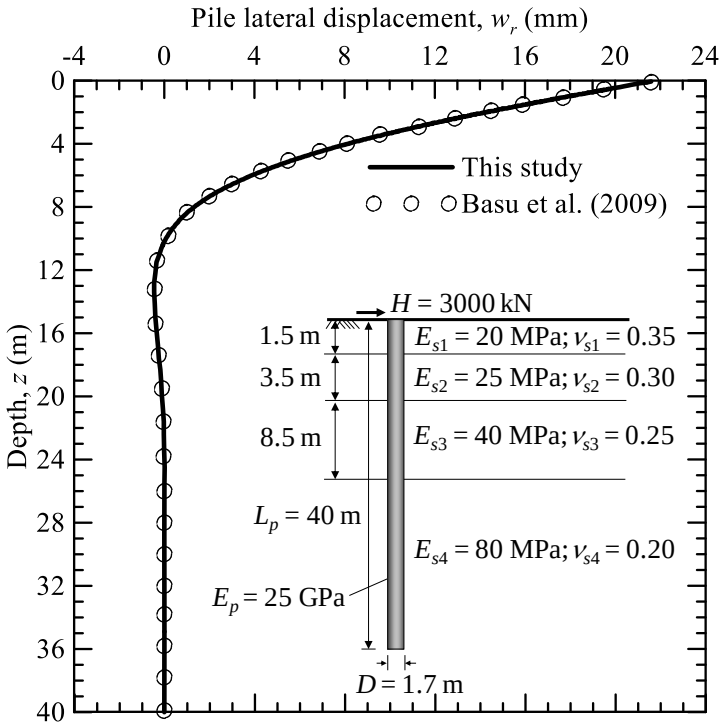

(b)

Figure 3.4 Comparison with previous studies for a foundation subjected to a pure lateral load: (a) D = 0.6 m and L_p = 15 m and (b) D = 1.7 m and L_p = 40 m

3.3.2 Torsional analysis

Misra et al. (2014) developed closed-form solutions of the angle of twist and torque for a foundation in multilayered elastic soil subjected to a pure torque using the method of initial parameters. We compare results from our analysis against those from Misra et al.'s solution for two example cases they reported.

The first example considers a drilled shaft, 1.5 m in diameter and 10 m long (L_p/D = 6.7), with shear modulus G_p = 9.6 GPa (equivalent to E_p = 25 GPa and ν_p = 0.3), embedded in a two-layered soil profile. The first layer extends from ground surface to a depth of 5 m with the elastic constants E_{s1} = 25 MPa and ν_{s1} = 0.40, and the second layer extends to great depth with E_{s2} = 100 MPa and ν_{s2} = 0.20. The applied torque T at the foundation head is 100 kN-m with zero lateral load (*i.e.*, H = 0).

The second example considers a drilled shaft, 1.0 m in diameter and 30 m long (L_p/D = 30), embedded in a four-layered soil profile. The top three layers are located over 0-5 m, 5-10 m, and 10-20 m below the ground surface. The fourth layer extends from the bottom of the third layer to great depth. The elastic constants of the four layers are as follows: E_{s1} = 25 MPa and ν_{s1} = 0.45 for Layer 1, E_{s2} = 50 MPa and ν_{s2} = 0.35 for Layer 2, E_{s3} = 75 MPa and ν_{s3} = 0.30 for Layer 3, and E_{s4} = 100 MPa and ν_{s4} = 0.25 for Layer 4. The shear modulus G_p is 9.6 GPa, and torque T = 100 kN-m is applied at the foundation head with zero lateral load.

The angles of twist ψ_p versus depth z obtained from our analysis and the study by Misra et al. (2014) for the two examples are presented in Figure 3.5, and they show excellent agreement (note that ψ_p beneath the foundation base was not reported in Misra et al.'s study and hence not presented in Figure 3.5). Both examples suggest that the angle of twist decreases with increasing depth because more soils resist to the applied torque as the depth increases. Due to its high embedment depth ratio of L_p/D = 30 for the foundation in the four-layered soil deposit, an angle of twist becomes zero at the foundation base (see Figure 3.5b). However, the foundation with L_p/D = 6.7 in the two-layered deposit show more rigid behavior than the foundation with L_p/D = 30, leading to

a non-zero value of angle of twist at the foundation base; but ψ_p quickly diminishes through the soil beneath the foundation base (see Figure 3.5a).

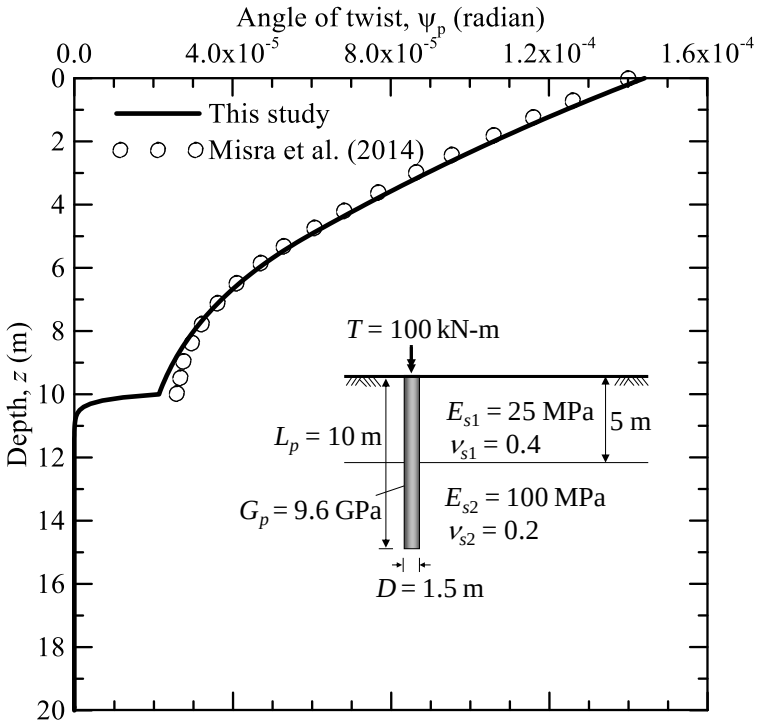

(a)

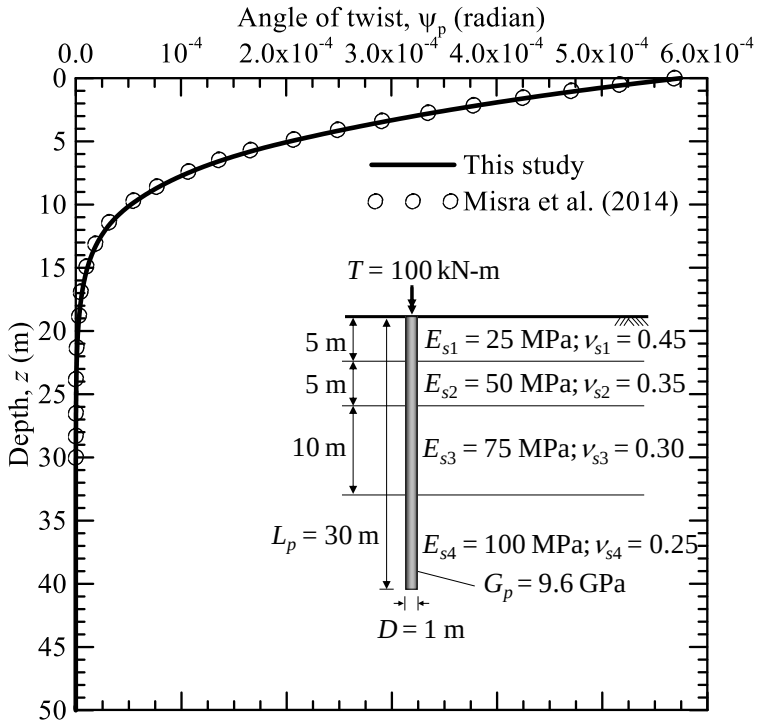

(b)

Figure 3.5 Comparison with previous studies for a foundation subjected to a pure torsion: (a) two-layered deposit and (b) four-layered deposit

3.4 Future studies

The new analysis model developed in this chapter is valid for linear elastic soils only. Furthermore, the short duration of the project prohibited a full implementation of solution algorithm under the combined loading. However, given that our analysis model shows very good agreement with previous studies and FEA under individual loading components, the solution algorithm developed in this study can be fully implemented and thorough benchmark runs can be performed as future studies. Furthermore, this study can be regarded as the groundwork for more advanced analyses such as nonlinear analysis that considers degradation of soil modulus using a piecewise-linear approach. Also, because the new analysis model is applicable for a multilayered soil, a systematic parametric study can be performed to investigate the soil layering effect and optimize foundation design.

CHAPTER 4. SUMMARY AND CONCLUSIONS

In this study, we performed a nonlinear finite element analysis (FEA) for a circular foundation in a homogeneous clay under combined loading of a lateral load and a torque using Tresca model. Failure envelopes in a lateral-torsional loading plane were obtained from FEA, and the effect of a torsional load on the lateral capacity of a circular foundation was quantified as a function of torque-to-lateral load ratio. We further developed a novel, linear-elastic analysis model for a circular foundation, embedded in a multilayered soil, under concurrent application of lateral and torsion loads using energy principles and variational calculus.

To determine collapse loads, the displacement-controlled swipe loading path method was employed in FEA. As a validation of the finite element model, the results from FEA under each individual component of load were compared against previous studies and theoretical values, which showed an excellent agreement. Analysis results under combined loading were presented in the form of failure envelopes with various embedment depth ratios (L_p/D) using four definitions of ultimate lateral capacity. For foundations with embedment depth ratios less than 3, the normalized failure envelopes fell on top of each other regardless of how lateral ultimate capacity was defined, suggesting that a single failure envelope can be used for short foundations. However, as the embedment depth ratio increased, the normalized failure envelopes deviated from each other and the use of single failure envelope was not justified for L_p/D = 10.

Results from FEA clearly showed that lateral capacity was reduced by the concurrent application of torsion. Such reduction effects were quantified as a function of torque-to-lateral load ratio and presented in the form of design charts. Analysis results further indicated that the lateral capacity could be reduced to 63% of maximum value under a torque-to-lateral load ratio of about 0.58 m for the soil condition and the range of torque-to-lateral load ratio (T/H) considered in this study. Whether the lateral capacity will continue to decrease beyond the range of T/H considered in this study is unknown at

this time and warrants further investigation. Typical ranges of T/H for various transportation infrastructures will need to be examined in future studies as well.

We also derived governing differential equations for a circular foundation, embedded in a layered soil, subjected to a combination of torsional and lateral loads based on energy principles and variational calculus. For the foundation-soil system under concurrent application of lateral and torsional loads, a total of six interdependent differential equations were obtained. We further developed a numerical algorithm to solve the interdependent differential equations using an iterative scheme and tested the algorithm under individual loading components. The results from our analysis model under individual loading components showed very good agreements with those from previous studies and FEA.

The solution algorithm developed in this study can be fully implemented for combined loading case and thorough benchmark runs can be performed as future studies. Furthermore, the analysis model developed in this study can be regarded as the groundwork for more advanced models such as nonlinear analysis model that considers degradation of soil modulus using a piecewise-linear approach. Also, because the new analysis model is applicable for a multilayered soil, a systematic parametric study can be performed to investigate the soil layering effect and optimize foundation design.

REFERENCES

ASCE (2013). Minimum Design Loads for Buildings and Other Structures (ASCE/SEI 7-10). American Society of Civil Engineers, Reston, VA.

Basu, D., Salgado, R., and Prezzi, M. (2009). “A continuum-based model for analysis of laterally loaded piles in layered soils.” Geotechnique, Vol. 59, No. 2, pp. 127-140

Beneberu, E., Goode, J., and Yazdani, N. (2014). “Computational fluid dynamics application for design of highway sign support structures.” International Journal of Civil and Structural Engineering, Vol. 5, No. 2, pp.101-111

Dassault Systèmes. (2016), Abaqus analysis user’s manual. Simulia Corp, Providence, RI, USA

Deng, W. and Carter, J., P. (1999). "Analysis of suction caissons in uniform soils subjected to inclined uplift loading", Report No. R798, Department of Civil Engineering, Sydney University, Australia

FEMA (2007). Design Guide for Improving Critical Facility Safety from Flooding and High Winds (FEMA 543). Federal Emergency Management Agency

Fan, Q. and Meng, X. (2011). “Failure Envelope of Pipe Pile Foundation under Combined Loading.” Proceedings of GeoHunan 2011 International Conference, pp. 109-119, https://doi.org/10.1061/47631(410)13

Gourvenec, S. and Randolph, M. (2003). “Effect of strength non-homogeneity on the shape of failure envelopes for combined loading of strip and circular foundations on clay.” Geotechnique, Vol. 53, pp. 575-586.

Guo. W, Chow, Y. K., Randolph, M. F. (2007). “Torsional piles in two-layered nonhomogeneous soil.” International Journal of Geomechanics, Vol. 7, No. 6, pp.410–422.

Guo, W. D., Randolph, M. F. (1996). “Torsional piles in non-homogeneous media.” Computers and Geotechnics; Vol. 19, No. 4, pp. 265–287.

Hache, R. A. G, Valsangkar, A. J. (1988). “Torsional resistance of single pile in layered soil.” Journal of Geotechnical Engineering, Vol. 114, No. 2, pp. 216–220.

Hu, Z., McVay, M., Bloomquist, D., Herrera, R., and Lai, P. (2006). “Influence of Torque on Lateral Capacity of Drilled Shafts in Sands.” Journal of Geotechnical and Geoenvironmental Engineering, Vol. 132, No. 4., pp. 456-464

IBC (2015). International Building Code: Chapter 16 Structural Design. http://codes.iccsafe.org/app/book/content/2015-I-Codes/2015%20IBC%20HTML/Chapter%2016.html, accessed on 10/20/2016

Lee, J.K., Jeong, S., and Shang, J.Q. (2016). “Undrained bearing capacity of ring foundations on two-layered clays.” Ocean Engineering, Vol. 119, pp. 47-57.

Li, Q., Stuedlein, A. W., and Barbosa, A. R. (2017). “Torsional Load Transfer of Drill Shaft Foundations.” Journal of Geotechnical and Geoenvironmental Engineering, Vol. 143, No. 8, 04017036

McVay, M. C., Herrera, R., and Hu, Z. (2003). “Determine Optimum Depths of Drilled Shafts Subject to Combined Torsional and Lateral Loads Using Centrifuge Testing.” A Draft Final Report submitted to Florida Department of Transportation, University of Florida

Misra, A., Saggu, R., Basu, D., and Chakraborty, T. (2014). “Analysis of pile subjected to torsion in multi-layered soil.” International Journal for Numerical and Analytical Methods in Geomechanics, Vol. 38, pp. 475-492

Randolph, M. F. (1981). “Piles Subjected to Torsion.” Journal of the Geotechnical Division, Vol. 107, No. GT8, pp. 1095-1111

Salgado, R., Seo, H., and Prezzi, M. (2013). “Variational Elastic Solution for Axially Loaded Piles in Multilayered Soil.” International Journal for Numerical and Analytical Methods in Geomechanics, Vol. 37, No. 4, pp. 423-440

Seo, H., Basu, D., Prezzi, M., and Salgado, R. (2009). “Load-Settlement Response of Rectangular and Circular Piles in Multilayered Soil.” Journal of Geotechnical and Geoenvironmental Engineering, Vol. 135, No. 3, pp. 420-430

Tan, F.S. (1990). Centrifuge and theoretical modelling of conical footings on sand. PhD thesis. University of Cambrigde, Cambrigde.

Taiebat, H. A. and Carter, J. P. (2004). “Effects of Torsion on Caisson Capacity in Clay.” Proceedings of 9th Austrailia New Zealand Conference on Geomechanics, Vol. 1, pp. 130-136

Thiyyakkandi, S., McVay, M., Lai, P., and Herrera, R. (2016). “Full-scale coupled torsion and lateral response of mast arm drilled shaft foundations.” Canadian Geotechnical Journal, Vol. 53, pp. 1928-1938

Vallabhan, C. V. G. and Mustafa, G. (1996). “A new model for the analysis of settlement of drilled piers.” International Journal for Numerical and Analytical Methods in Geomechanics, 20, pp. 143-152

Vlasov, V.Z., and Leont’ev, N. N. (1966). “Beams, plates and shells on elastic foundations.” NTIS Accession No. N67-14238, Israel Program for Scientific Translations, Jerusalem, Israel.

Vulpe, C., Gourvenec, S., and Power, M. (2014). “A generalised failure envelope for undrained capacity of circular shallow foundations under general loading.” Geotechnique Letters, Vol. 4, pp. 187-196.

Zhang, L. (2010). “Nonlinear Analysis of Torsionally Loaded Piles in a Two-Layered Soil Profile.” International Journal of Geomechanics, Vol.10, No. 2, pp. 65-73